Article

STING cyclic dinucleotide sensing originated in bacteria

https://doi.org/10.1038/s41586-020-2719-5

Received: 2 May 2020

Accepted: 26 August 2020

Published online: 2 September 2020

Check for updates

Benjamin R. Morehouse[1,2], Apurva A. Govande[1,2], Adi Millman[3], Alexander F. A. Keszei[4], Brianna Lowey[1,2], Gal Ofir[3], Sichen Shao[4], Rotem Sorek[3] & Philip J. Kranzusch[1,2,5]✉

Stimulator of interferon genes (STING) is a receptor in human cells that senses foreign cyclic dinucleotides that are released during bacterial infection and in endogenous cyclic GMP–AMP signalling during viral infection and anti-tumour immunity[1–5]. STING shares no structural homology with other known signalling proteins[6–9], which has limited attempts at functional analysis and prevented explanation of the origin of cyclic dinucleotide signalling in mammalian innate immunity. Here we reveal functional STING homologues encoded within prokaryotic defence islands, as well as a conserved mechanism of signal activation. Crystal structures of bacterial STING define a minimal homodimeric scaffold that selectively responds to cyclic di-GMP synthesized by a neighbouring cGAS/DncV-like nucleotidyltransferase (CD-NTase) enzyme. Bacterial STING domains couple the recognition of cyclic dinucleotides with the formation of protein filaments to drive oligomerization of TIR effector domains and rapid NAD^+ cleavage. We reconstruct the evolutionary events that followed the acquisition of STING into metazoan innate immunity, and determine the structure of a full-length TIR–STING fusion from the Pacific oyster *Crassostrea gigas*. Comparative structural analysis demonstrates how metazoan-specific additions to the core STING scaffold enabled a switch from direct effector function to regulation of antiviral transcription. Together, our results explain the mechanism of STING-dependent signalling and reveal the conservation of a functional cGAS–STING pathway in prokaryotic defence against bacteriophages.

Bioinformatics analysis of the bacteriophage defence islands of prokaryotes has revealed a group of divergent genes that encode the first known candidate proteins outside of metazoan innate immunity that have predicted homology to STING[10] (Extended Data Fig. 1a). To understand a potential role for STING in bacterial signalling, we determined 1.8 Å and 2.8 Å crystal structures of candidate homologues from Flavobacteriaceae sp. (Integrated Microbial Genomes (IMG) gene identifier 2624319773) and *Capnocytophaga granulosa* (IMG gene identifier 2541326748), respectively (Supplementary Table 1). The bacterial structures exhibit clear homology to the cyclic-dinucleotide-binding domain of human STING and confirm that this subset of defence island proteins represent newly identified prokaryotic members of the STING family of receptors (Fig. 1a). Flavobacteriaceae sp. STING (FsSTING) and *Capnocytophaga granulosa* STING (*Cg*STING) adopt a canonical V-shaped, homodimeric architecture with a hydrophobic α-helix stem that is similar to that observed in all structures of metazoan STING proteins[6–9] (Fig. 1b). We determined the FsSTING structure in complex with 3′–5′/3′–5′-cyclic GMP–AMP (3′,3′-cGAMP), which confirms that bacterial STING proteins are functional cyclic dinucleotide receptors (Fig. 1a). Alignment of the FsSTING–3′,3′-cGAMP complex with apo *Cg*STING revealed that cyclic dinucleotide binding induces rotation of the monomeric domains and results in the closure of β-strands 2 and 3 to form a lid that seals a central cyclic-dinucleotide-binding pocket (Fig. 1a, Extended Data Fig. 1b–d). Although the overall architecture is conserved with metazoan STING, bacterial STING proteins are 20% smaller and notably compact. Metazoan insertions into the core bacterial STING fold include an extension within the β-strand lid domain, the addition of a terminal α-helix required for induction of autophagy, and an unstructured C-terminal tail that contains motifs required for the recruitment of kinases and transcription factors in vertebrates[11–14] (Fig. 1b).

We analysed bacterial STING sequences and found that 84% are encoded in cyclic oligonucleotide-based signalling system (CBASS) immunity operons[10] (Fig. 2a). Similar to cGAS-dependent sensing of viral replication in human cells[4,5], CBASS immunity relies on the activation of a CD-NTase enzyme to initiate a second messenger-dependent antiviral effector response[10,15,16]. We cloned the Flavobacteriaceae sp. CD-NTase *CdnE* (CD-NTase in clade E) that is adjacent to FsSTING, and observed that FsCdnE specifically synthesizes the cyclic dinucleotide cyclic di-GMP (c-di-GMP)[15] (Fig. 2b). FsCdnE is constitutively active in vitro, consistent with an emerging model in which CBASS immune systems may function through inhibitory molecules that repress CD-NTase activation in the absence of phage infection[10,15–17]. We confirmed the exclusive production of c-di-GMP by CdnE enzymes

[1]Department of Microbiology, Harvard Medical School, Boston, MA, USA. [2]Department of Cancer Immunology and Virology, Dana-Farber Cancer Institute, Boston, MA, USA. [3]Department of Molecular Genetics, Weizmann Institute of Science, Rehovot, Israel. [4]Department of Cell Biology, Harvard Medical School, Boston, MA, USA. [5]Parker Institute for Cancer Immunotherapy, Dana-Farber Cancer Institute, Boston, MA, USA. ✉e-mail: philip_kranzusch@dfci.harvard.edu

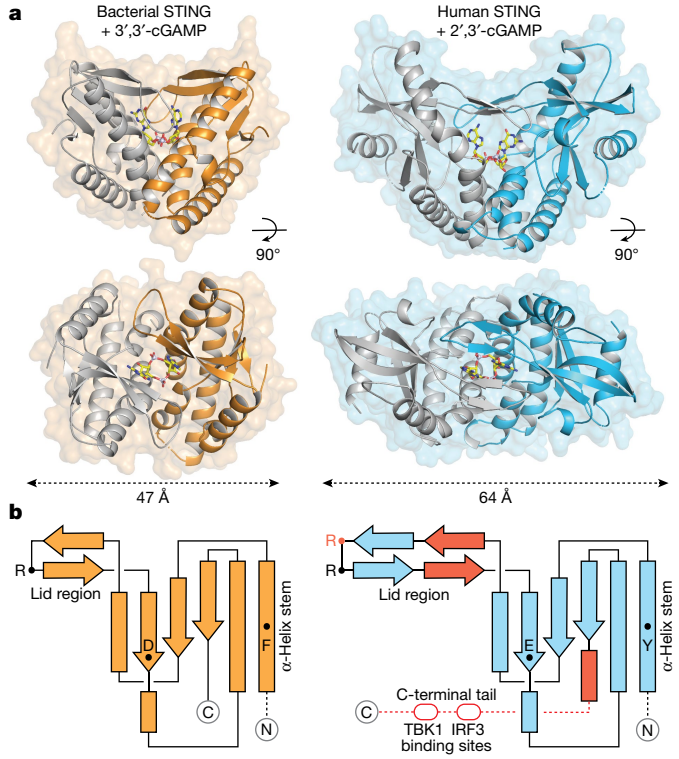

Fig. 1 | Structure of bacterial STING, and definition of metazoan-specific insertions. a, Crystal structure of a STING receptor from a bacterial species of the family Flavobacteriaceae (orange) in complex with the cyclic dinucleotide 3′,3′-cGAMP. The FsSTING–3′,3′-cGAMP structure demonstrates a conserved mechanism for sensing cyclic dinucleotides that is shared between bacteria and human cells, and allows direct comparison with the human STING–2′,3′-cGAMP complex (Protein Data Bank (PDB) code 4KSY) (blue). For clarity, one monomer of each homodimer is depicted in grey. **b**, STING topology diagrams denoting α-helices (rectangles), β-strands (arrows) and residues important for ligand recognition (FsSTING: F92, D169 and R153; human STING: Y167, E260, R232 (in red) and R238). Bacterial STING receptors reveal a minimal protein architecture that is required for cyclic dinucleotide sensing and allow direct definition of the structural insertions (red) in metazoan STING sequences that are required for signalling in animal cells.

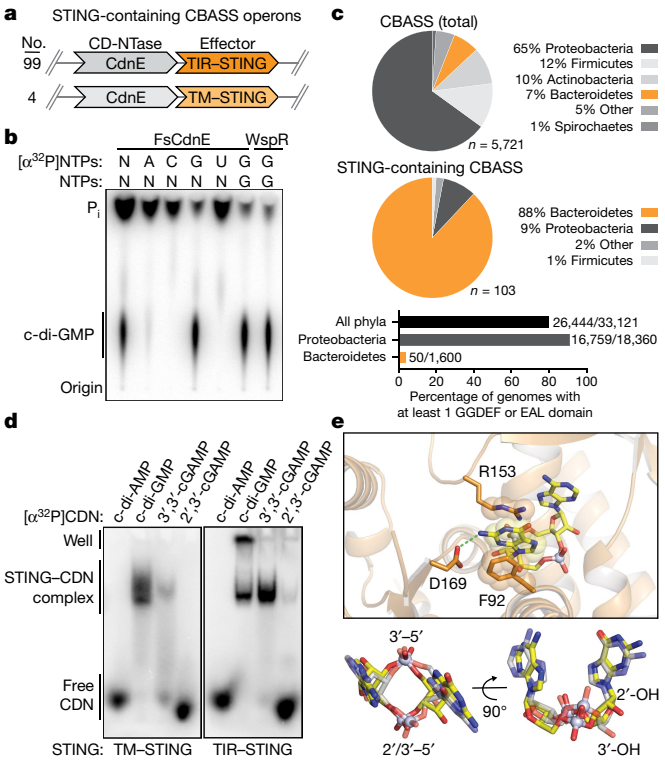

Fig. 2 | Bacterial STING systems signal through the 3′–5′-linked nucleotide second messenger c-di-GMP. a, Schematic of STING-containing CBASS prokaryotic defence operons. STING is encoded downstream of a clade-E CD-NTase nucleotide second messenger synthase (CdnE) and exists as a fusion protein appended to TIR or transmembrane (TM) effector modules with 99 and 4 sequences found, respectively. **b**, Thin-layer chromatography analysis of nucleotide second messenger synthesis by FsCdnE. CdnE enzymes in STING-containing CBASS operons require GTP for catalysis and specifically synthesize the 3′–5′-linked product c-di-GMP. Control c-di-GMP synthesis reactions were performed with the GGDEF enzyme WspR from *Pseudomonas aeruginosa*. N, all four radiolabelled NTPs; P_i, inorganic phosphate. Data are representative of three independent experiments. **c**, Analysis of the genomic context of all STING-containing CBASS operons. STING-containing CBASS operons in bacteria occur mainly in Bacteroidetes (top). Sequenced Bacteroidetes genomes are generally devoid of canonical GGDEF and EAL c-di-GMP signalling domains (bottom), and 97 out of 99 STING-containing bacteria lack any other predicted c-di-GMP signalling component. Loss of canonical c-di-GMP signalling provides an explanation for co-option of c-di-GMP as a CD-NTase immune signal. Numbers alongside the bar graphs denote the number of genomes that contain at least one gene with a GGDEF or EAL domain out of the total number of genomes in the analysed database. **d**, Electrophoretic mobility shift assay monitoring the formation of a bacterial STING–cyclic dinucleotide (CDN) complex. Bacterial TM–STING and TIR–STING proteins preferentially recognize c-di-GMP and exhibit weaker affinity for 3′,3′-cGAMP. Bacterial STING receptors are unable to recognize the mammalian second messenger 2′,3′-cGAMP. TM–STING (*Roseivirga ehrenbergii*, ΔTM) and TIR–STING (*Sphingobacterium faecium*, full-length). Data are representative of three independent experiments. **e**, Enlarged cutaway of the cyclic-dinucleotide-binding pocket in the FsSTING–3′,3′-cGAMP structure. Top, FsSTING makes sequence-specific contacts to the guanine base, consistent with preferential c-di-GMP recognition. Bottom, bacterial STING recognizes 3′,3′-cGAMP (yellow) in a compact conformation similar to 2′,3′-cGAMP (grey) in complex with human STING (PDB 4KSY).

encoded within three additional divergent STING-containing CBASS operons (Extended Data Figs. 2a, 3a–c). In addition, we determined 1.5 Å and 2.3 Å crystal structures for two CdnE homologues, which revealed an active enzyme conformation and unique substitutions in the nucleobase acceptor pocket that are consistent with adaptation for c-di-GMP synthesis[15] (Extended Data Figs. 2b, 3d–f). c-di-GMP is a common nucleotide second messenger that is used to regulate bacterial growth and intracellular signalling[18], and it is therefore difficult to conceive how bacteria could distinguish these functions of c-di-GMP from the induction of CBASS immunity that results in rapid bacterial death[10,16,17]. To explain the unexpected role of c-di-GMP in CBASS immunity, we analysed the genomic context of all STING-containing CBASS operons and discovered that these systems are encoded almost exclusively in bacteria that are devoid of canonical GGDEF and EAL c-di-GMP signalling domains, which suggests complete co-option of normal c-di-GMP function for a role in STING activation (Fig. 2c).

Bacterial STINGs bind c-di-GMP with nanomolar affinity and exhibit a clear preference for canonical 3′–5′-linked cyclic dinucleotides (Fig. 2d, Extended Data Fig. 4a, b). In the FsSTING–3′,3′-cGAMP structure, the cyclic dinucleotide backbone is coordinated with N91 and N172, and each nucleobase is sandwiched between a stacking interaction formed with F92 and R153 (Fig. 2e). In agreement with the strong preference of bacterial STING for c-di-GMP, a universally conserved D169 residue reads out the guanosine nucleobase by making a sequence-specific contact to the N2 position (Fig. 2e). Using mutational analysis, we verified the importance of residues in the cyclic-dinucleotide-binding pocket of STING and confirmed that conserved nucleobase contacts are required for the recognition of c-di-GMP (Extended Data Figs. 5, 6a–e). Human

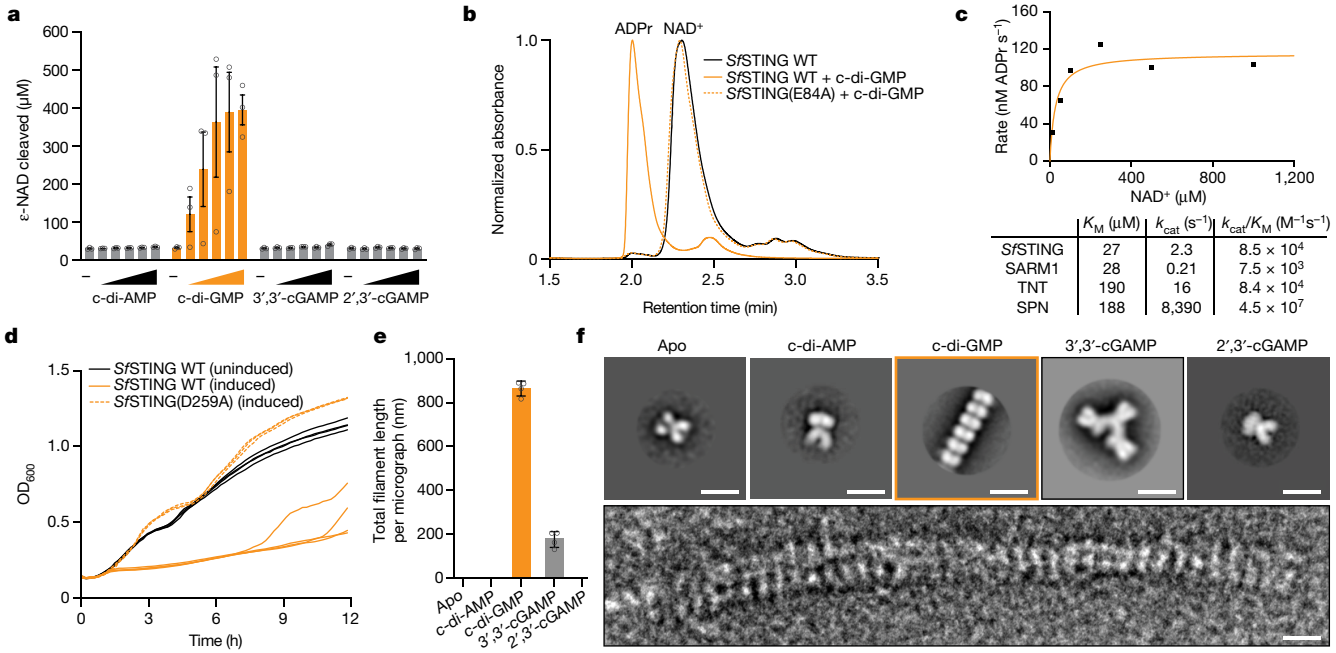

Fig. 3 | Cyclic dinucleotide recognition controls bacterial STING oligomerization and TIR NAD+ cleavage activity. a, Analysis of *S. faecium* TIR–STING (*Sf*STING) NAD^+ cleavage activity using the fluorescent substrate ε-NAD. TIR–STING activity is potently stimulated in the presence of c-di-GMP (0, 5, 10, 15 and 20 nM, and 20 μM). Data are mean ± s.e.m. for $n = 3$ biological replicates. **b**, High-performance liquid chromatography analysis of TIR–STING NAD^+ cleavage. *Sf*STING cleaves NAD^+ into the products ADPr and NAM, and activity is strictly dependent on the TIR active-site residue E84. Data are representative of three independent experiments. WT, wild type. **c**, Quantification of *Sf*STING activity and comparison with the previously characterized NADase and glycosyl hydrolase enzymes human SARM1[32], *Mycobacterium tuberculosis* TNT[33] and *Streptococcus pyogenes* SPN[34]. Data are mean for $n = 2$ independent replicates and are representative of 3 independent experiments. **d**, Analysis of *Sf*STING toxicity in *E. coli* cells expressing normal c-di-GMP signalling enzymes. Expression of *Sf*STING from an arabinose-inducible promoter (induced) results in a potent growth-arrest phenotype. Toxicity is lost with a D259A mutation to the *Sf*STING cyclic-dinucleotide-binding domain that inhibits c-di-GMP recognition. Each line represents the average of two technical replicates for each of four separately outgrown colonies. Data are representative of two independent experiments. OD_{600}, optical density at 600 nm. **e**, Negative-stain electron microscopy analysis and quantification demonstrates that *Sf*STING forms stable filaments only in the presence of c-di-GMP. Data are mean ± s.d. for quantification of $n = 4$ groups of 10 micrograph images. **f**, Electron microscopy analysis of *Sf*STING filament formation. Top, 2D class averages demonstrate that *Sf*STING forms well-ordered filaments in the presence of c-di-GMP and smaller fragmented assemblies in the presence of 3′,3′-cGAMP. Bottom, *Sf*STING–c-di-GMP filaments can be >30 nm in length. Two dimensional class averages were derived from particles selected from 75 micrographs for each condition. Scale bars, 100 Å.

STING does not form prominent sequence-specific contacts with cyclic dinucleotides. Instead, the R232 residue in human STING makes an additional contact to the phosphodiester backbone and is critical for high-affinity recognition of the mammalian cGAS product 2′–5′/3′–5′ cGAMP (2′,3′-cGAMP)[7,19]. A notable feature of bacterial STING receptors is an inability to recognize mammalian 2′,3′-cGAMP (Fig. 2d, Extended Data Fig. 4a, b). Cyclic dinucleotides occupy a similar, compact conformation in both bacterial STING and human STING, but in bacterial STING the R232-equivalent position (R151) is flipped outwards and does not contact the cyclic dinucleotide backbone (Extended Data Fig. 1e). Furthermore, a universally conserved T173 residue in bacterial STING, located beneath the cyclic-dinucleotide-binding pocket, reduces the space that would be necessary to accommodate a free 3′-OH within 2′,3′-cGAMP (Extended Data Fig. 1f). We observed that bacterial STING is over 1,000× more sensitive to c-di-GMP than a synthetic analogue with a 2′–5′ linkage (2′,3′-c-di-GMP) (Extended Data Fig. 5g), further confirming the strict specificity of bacterial STING for 3′–5′-linked cyclic dinucleotides.

Activation of CBASS immunity induces bacterial growth arrest or cell death to destroy virally infected cells and limit the propagation of phages[10,16,17]. Bacterial STING domains occur primarily as fusions to a Toll/interleukin-1 receptor (TIR) adaptor domain, or more rarely are appended to predicted transmembrane segments (Fig. 2a, Extended Data Fig. 1a). TIR domains can function as β-nicotinamide adenine dinucleotide (NAD^+) hydrolases in plant and animal immunity[20–22]. We therefore tested a full-length TIR–STING fusion from *Sphingobacterium faecium* (*Sf*STING) (IMG gene identifier 2735805876) for catalytic function, and observed rapid hydrolysis of NAD^+ to nicotinamide and adenine diphosphate-ribose (Fig. 3a, b, Extended Data Fig. 5a–d). *Sf*STING potently responds to c-di-GMP and weakly to 3′,3′-cGAMP, and catalysis is abolished by mutating a conserved TIR glutamic acid residue in the active site (Fig. 3b, Extended Data Fig. 6f, g). Activation of bacterial TIR–STING requires lower than 100 nM c-di-GMP, and results in cleavage of NAD^+ at 10× the rate observed for plant and animal TIR proteins involved in immune defence (Fig. 3c, Extended Data Fig. 5h, i). We expressed *Sf*STING in *Escherichia coli* cells that synthesize c-di-GMP and observed potent growth inhibition (Fig. 3d). *Sf*STING-induced toxicity is lost with a D259A mutation that prevents c-di-GMP recognition, and can be partially overcome with nicotinamide supplementation (Fig. 3d, Extended Data Fig. 6h, i), which provides further support for a role for bacterial STING in CBASS-mediated immunity as a c-di-GMP-responsive NADase effector.

Recognition of cyclic dinucleotides drives bacterial STING oligomerization and the formation of ordered filaments that are readily observable with negative-stain electron microscopy (Fig. 3e, f, Extended Data Fig. 7). In the presence of activating c-di-GMP, *Sf*STING assembles into filaments that are typically 25–30 nm in length, and that exhibit four-fold symmetry and contain an ordered array of parallel-stacked homodimers (Fig. 3f, Extended Data Fig. 7j–l). Electron microscopy and biochemical analysis of *Sf*STING in the presence of the weak agonist

3′,3′-cGAMP reveals partial filament formation and STING complexes in a tetramer-like conformation, indicating that cyclic dinucleotide stabilization of STING tetramers is probably required to seed filament growth (Fig. 3e, f, Extended Data Fig. 7j–l). Higher-order oligomerization is a known requirement for TIR activation[21,22], and mutations to the *Sf*STING cyclic-dinucleotide-binding domain that disrupt c-di-GMP-induced oligomerization prevent activation of TIR–STING NAD^+ cleavage (Extended Data Fig. 6b, f, g). Filament formation by bacterial STING is consistent with a recently proposed model of human STING activation, in which parallel-stacking of STING homodimers initiates oligomerization and recruitment of the kinase TBK1[12,23]. Using the cryo-electron microscopy structure of chicken STING as a guide[9], we constructed a model of bacterial STING oligomerization and identified surfaces in the bacterial STING domain at the beginning of helix α2 and end of helix α4 that are predicted to mediate oligomerization (Extended Data Fig. 8a). Mutations to these surfaces do not disrupt c-di-GMP binding by *Sf*STING, but do prevent oligomerization into filaments (Extended Data Fig. 8b, c). In the absence of filament formation, all *Sf*STING NADase activity is lost (Extended Data Fig. 8d), which confirms that c-di-GMP-induced oligomerization is essential for TIR domain activation and effector function. These results define a core role of filament formation in STING activation and suggest that the primordial mechanism of STING signalling is cyclic-dinucleotide-dependent effector oligomerization.

Our high-resolution crystal structures of FsSTING and *Cg*STING allowed us to construct a structure-guided phylogenetic alignment of 103 bacterial and 492 metazoan STING proteins for comparative analysis of STING function and adaptation (Fig. 4a, Extended Data Figs. 9a, 10a). The distribution of STING is most consistent with a bacterial origin and acquisition into an early metazoan ancestor (Extended Data Fig. 10a). The distinct residues of the cyclic-dinucleotide-binding pocket that are required for preferential recognition of c-di-GMP or 2′,3′-cGAMP are fixed and nearly exclusive to bacterial or metazoan STING sequences. Strict kingdom-specific conservation further supports 2′,3′-cGAMP as the dominant functional ligand throughout metazoan STING signalling, and suggests that a clear transition occurred from c-di-GMP signalling in bacteria to noncanonical cyclic dinucleotide signalling in animals[8,11,24] (Extended Data Fig. 10b). We identified several instances of invertebrate metazoan TIR–STING fusions with a predicted architecture similar to that of bacterial STING, including within oyster genomes that have previously been noted to encode marked expansions of innate immune receptors and predicted CD-NTase enzymes[8,24,25]. To further understand the adaptation of STING to signalling in animal cells, we determined a 2.4 Å crystal structure of metazoan TIR–STING from the Pacific oyster *C. gigas* (oyster TIR–STING). The structure of the full-length oyster TIR–STING reveals a domain-swapped configuration with a linker region that intertwines to connect the appended TIR effector module with the STING dimerization α-helix stem (Fig. 4b). We next determined a 2.9 Å crystal structure of oyster TIR–STING in complex with 2′,3′-cGAMP, confirming the phylogenetic analysis of strict retention of 2′,3′-cGAMP-interacting residues in invertebrate metazoan STING receptors (Fig. 4b, Extended Data Figs. 9f, 10b). Distinct from a recent cryo-electron microscopy analysis of full-length human STING with the N-terminal transmembrane domain, no 180° rotation is observed in the linker that connects the oyster STING and TIR domains in the presence of 2′,3′-cGAMP[9]. Instead, closure of oyster STING around 2′,3′-cGAMP re-aligns intermonomer contacts between the adjacent STING and TIR domains, inducing a downward 4° rotation in TIR domain orientation (Fig. 4b). We did not observe oyster TIR–STING catalytic NAD^+ cleavage activity in the presence of cyclic dinucleotides, which suggests additional requirements for enzyme activation or that reorientation of the TIR domain may instead facilitate protein–protein interactions similar to the signalling adaptor function of TIR domains in human MyD88 and TRIF[26] (Extended Data Fig. 9b–h). These results further explain the adaptation of STING in metazoans and provide a molecular mechanism for how cyclic dinucleotide sensing by STING is structurally communicated to appended effector modules.

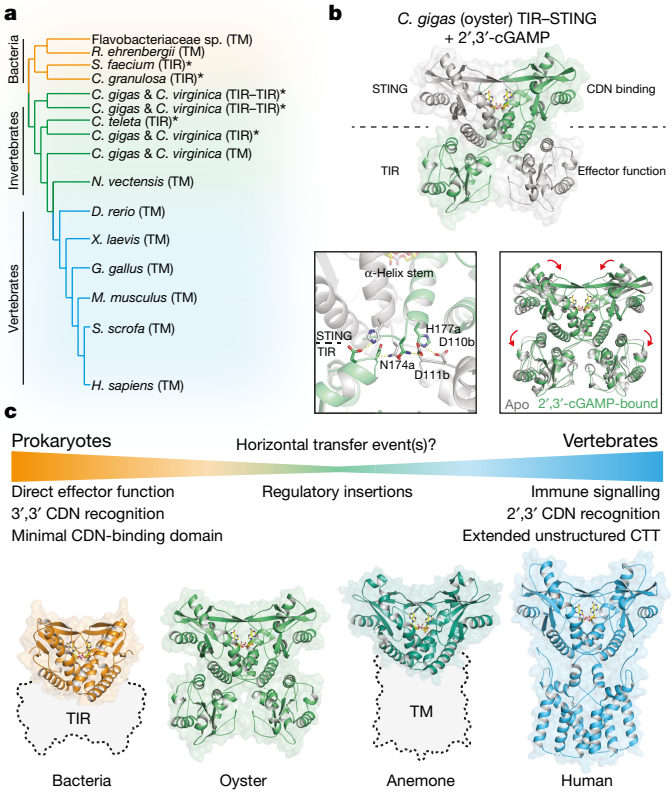

Fig. 4 | Structural basis of STING adaptation for signalling regulation. a, Schematic derived from a structure-guided alignment of all known bacterial and metazoan STING sequences. Black stars denote TIR–STING fusions encoded in bacterial and metazoan genomes. Oysters encode several TIR–STING variants, including genes predicted to contain multiple TIR domains (TIR–TIR). **b**, Crystal structure of the full-length *C. gigas* (oyster) TIR–STING receptor (GenBank sequence XP_011430837.1) in complex with 2′,3′-cGAMP. Top, oyster TIR–STING adopts a domain-swapped conformation with TIR domains appended across a central dimeric axis. Bottom left, 2′,3′-cGAMP recognition results in new interactions between the STING domain α-helix stem of one monomer and the TIR domain of the other monomer. Bottom right, ligand binding induces STING-domain lid closure and a downward rotation that repositions the appended TIR domains. **c**, Comparative structural analysis of STING adaptation suggests a model for the origin of cyclic dinucleotide sensing in innate immunity. STING evolved as a c-di-GMP sensor in prokaryotic bacteriophage defence, and acquisition in early metazoan cells may have allowed recognition of bacterial cyclic dinucleotides. Metazoan-specific structural insertions adapted STING for recognition of endogenous 2′,3′-cGAMP signalling and enabled antiviral and anti-tumour immune signalling in vertebrate cells. Structures shown: bacterial STING–3′,3′-cGAMP (FsSTING), oyster STING–2′,3′-cGAMP (*C. gigas*), sea anemone STING–2′,3′-cGAMP (*Nematostella vectensis* PDB 5CFQ), human STING–2′,3′-cGAMP (*H. sapiens* PDB 6NT5, modelled with 6NT7). CTT, C-terminal tail.

Our data define a conserved mechanism of STING-dependent signalling that is shared by bacteria and human cells, and support a unified model to explain the emergence of cyclic dinucleotide sensing in animal innate immunity[8,11,24] (Fig. 4c). Bacterial STING proteins function as c-di-GMP receptors that control the oligomerization-dependent activation of appended effector domains, and are frequently encoded in the genomes of species in Bacteroidetes that grow as commensals enriched in human and animal microbiota[27]. Notably, c-di-GMP was the first ligand of human STING to be discovered[3], and the recognition of bacterial cyclic dinucleotides by human STING is critical for the immune detection of intracellular pathogens such as *Listeria*

monocytogenes[28–30]. Acquisition of STING as a c-di-GMP receptor could therefore provide an immediate selective advantage that enabled animal cells to sense intracellular bacteria through detection of essential cyclic dinucleotide second messengers that are conserved in prokaryotes. Our structural analysis defines mutations of the cyclic-dinucleotide-binding pocket that adapted metazoan STING for recognition of endogenous 2′,3′-cGAMP signalling, and explains how the emergence of metazoan-specific insertions enabled autophagy and effector responses dependent on type I interferon. Together with the previous identification of diverse cGAS homologues and 2′–5′-linked signals in prokaryotic antiviral immunity[10,15,17,31], the functional conservation of STING in bacteria reveals that each of the core protein components that define human cGAS–STING signalling arose from an ancient mechanism of defence against bacteriophages.

Online content

Any methods, additional references, Nature Research reporting summaries, source data, extended data, supplementary information, acknowledgements, peer review information; details of author contributions and competing interests; and statements of data and code availability are available at https://doi.org/10.1038/s41586-020-2719-5.

1. Ishikawa, H. & Barber, G. N. STING is an endoplasmic reticulum adaptor that facilitates innate immune signalling. *Nature* **455**, 674–678 (2008).
2. Zhong, B. et al. The adaptor protein MITA links virus-sensing receptors to IRF3 transcription factor activation. *Immunity* **29**, 538–550 (2008).
3. Burdette, D. L. et al. STING is a direct innate immune sensor of cyclic di-GMP. *Nature* **478**, 515–518 (2011).
4. Sun, L., Wu, J., Du, F., Chen, X. & Chen, Z. J. Cyclic GMP–AMP synthase is a cytosolic DNA sensor that activates the type I interferon pathway. *Science* **339**, 786–791 (2013).
5. Ablasser, A. & Chen, Z. J. cGAS in action: expanding roles in immunity and inflammation. *Science* **363**, eaat8657 (2019).
6. Ouyang, S. et al. Structural analysis of the STING adaptor protein reveals a hydrophobic dimer interface and mode of cyclic di-GMP binding. *Immunity* **36**, 1073–1086 (2012).
7. Zhang, X. et al. Cyclic GMP–AMP containing mixed phosphodiester linkages is an endogenous high-affinity ligand for STING. *Mol. Cell* **51**, 226–235 (2013).
8. Kranzusch, P. J. et al. Ancient origin of cGAS–STING reveals mechanism of universal 2′,3′ cGAMP signaling. *Mol. Cell* **59**, 891–903 (2015).
9. Shang, G., Zhang, C., Chen, Z. J., Bai, X. C. & Zhang, X. Cryo-EM structures of STING reveal its mechanism of activation by cyclic GMP–AMP. *Nature* **567**, 389–393 (2019).
10. Cohen, D. et al. Cyclic GMP–AMP signalling protects bacteria against viral infection. *Nature* **574**, 691–695 (2019).
11. Gui, X. et al. Autophagy induction via STING trafficking is a primordial function of the cGAS pathway. *Nature* **567**, 262–266 (2019).
12. Zhang, C. et al. Structural basis of STING binding with and phosphorylation by TBK1. *Nature* **567**, 394–398 (2019).
13. Zhao, B. et al. A conserved PLPLRT/SD motif of STING mediates the recruitment and activation of TBK1. *Nature* **569**, 718–722 (2019).
14. de Oliveira Mann, C. C. et al. Modular architecture of the STING C-terminal tail allows interferon and NF-κB signaling adaptation. *Cell Rep.* **27**, 1165–1175 (2019).
15. Whiteley, A. T. et al. Bacterial cGAS-like enzymes synthesize diverse nucleotide signals. *Nature* **567**, 194–199 (2019).
16. Ye, Q. et al. HORMA domain proteins and a Trip13-like ATPase regulate bacterial cGAS-like enzymes to mediate bacteriophage immunity. *Mol. Cell* **77**, 709–722 (2020).
17. Lowey, B. et al. CBASS immunity uses CARF-related effectors to sense 3′-5′- and 2′-5′-linked cyclic oligonucleotide signals and protect bacteria from phage infection. *Cell* **182**, 38–49 (2020).
18. Jenal, U., Reinders, A. & Lori, C. Cyclic di-GMP: second messenger extraordinaire. *Nat. Rev. Microbiol.* **15**, 271–284 (2017).
19. Gao, P. et al. Structure-function analysis of STING activation by c[G(2′,5′)pA(3′,5′)p] and targeting by antiviral DMXAA. *Cell* **154**, 748–762 (2013).
20. Essuman, K. et al. TIR domain proteins are an ancient family of NAD^+-consuming enzymes. *Curr. Biol.* **28**, 421–430 (2018).
21. Horsefield, S. et al. NAD^+ cleavage activity by animal and plant TIR domains in cell death pathways. *Science* **365**, 793–799 (2019).
22. Wan, L. et al. TIR domains of plant immune receptors are NAD^+-cleaving enzymes that promote cell death. *Science* **365**, 799–803 (2019).
23. Ergun, S. L., Fernandez, D., Weiss, T. M. & Li, L. STING polymer structure reveals mechanisms for activation, hyperactivation, and inhibition. *Cell* **178**, 290–301 (2019).
24. Margolis, S. R., Wilson, S. C. & Vance, R. E. Evolutionary origins of cGAS–STING signaling. *Trends Immunol.* **38**, 733–743 (2017).
25. Zhang, G. et al. The oyster genome reveals stress adaptation and complexity of shell formation. *Nature* **490**, 49–54 (2012).
26. Toshchakov, V. Y. & Neuwald, A. F. A survey of TIR domain sequence and structure divergence. *Immunogenetics* **72**, 181–203 (2020).
27. Wexler, A. G. & Goodman, A. L. An insider's perspective: Bacteroides as a window into the microbiome. *Nat. Microbiol.* **2**, 17026 (2017).
28. Woodward, J. J., Iavarone, A. T. & Portnoy, D. A. c-di-AMP secreted by intracellular *Listeria monocytogenes* activates a host type I interferon response. *Science* **328**, 1703–1705 (2010).
29. Dey, B. et al. A bacterial cyclic dinucleotide activates the cytosolic surveillance pathway and mediates innate resistance to tuberculosis. *Nat. Med.* **21**, 401–406 (2015).
30. Sixt, B. S. et al. The *Chlamydia trachomatis* inclusion membrane protein CpoS counteracts STING-mediated cellular surveillance and suicide programs. *Cell Host Microbe* **21**, 113–121 (2017).
31. Burroughs, A. M., Zhang, D., Schäffer, D. E., Iyer, L. M. & Aravind, L. Comparative genomic analyses reveal a vast, novel network of nucleotide-centric systems in biological conflicts, immunity and signaling. *Nucleic Acids Res.* **43**, 10633–10654 (2015).
32. Loring, H. S., Icso, J. D., Nemmara, V. V. & Thompson, P. R. Initial kinetic characterization of sterile alpha and Toll/interleukin receptor motif-containing protein 1. *Biochemistry* **59**, 933–942 (2020).
33. Tak, U. et al. The tuberculosis necrotizing toxin is an NAD^+ and $NADP^+$ glycohydrolase with distinct enzymatic properties. *J. Biol. Chem.* **294**, 3024–3036 (2019).
34. Ghosh, J., Anderson, P. J., Chandrasekaran, S. & Caparon, M. G. Characterization of *Streptococcus pyogenes* β-NAD^+ glycohydrolase: re-evaluation of enzymatic properties associated with pathogenesis. *J. Biol. Chem.* **285**, 5683–5694 (2010).

Methods

No statistical methods were used to predetermine sample size. The experiments were not randomized and investigators were not blinded to allocation during experiments and outcome assessment.

Phylogenetic distribution of STING-domain proteins in bacterial genomes

CBASS operons and STING proteins were taken from the list identified in refs. [10,35], supplemented by additional bacterial STING homologues identified using the 'top IMG homologue hits' function in the IMG database[36]. To assess the prevalence of c-di-GMP use in different phyla, Pfam annotation data of all genes in 38,167 bacterial and archaeal genomes were downloaded from the IMG database[36] in October 2017. Genomes were supplemented with 44 genomes manually identified with STING-containing operons that were absent from the October 2017 dataset. Genes annotated with the diguanylate cyclase GGDEF domain (pfam00990) or the diguanylate phosphodiesterase EAL domain (pfam00563) were counted for each phylum represented by at least 200 genomes in the database.

Protein expression and purification. Recombinant STING homologues were generated and purified as previously described[15,37]. In brief, synthetic DNA constructs (Integrated DNA Technologies) were cloned via Gibson assembly into a modified pET16 vector for expression of recombinant N-terminal 6×His-, 6×His–SUMO2, or 6×His–MBP–SUMO2 fusion proteins in BL21-CodonPlus(DE3)-RIL *E. coli* (Agilent). Transformed bacteria were grown overnight in MDG medium before inoculation in M9ZB medium for large-scale protein expression (2–3 × 1-l flasks, grown at 37 °C with 230 rpm shaking). Once M9ZB cultures reached OD_{600} of about 2.5, flasks were placed on ice for 20 min to slow bacterial growth. Cultures were induced with 500 μM final IPTG concentration and incubated at 16 °C for about 20 h at 230 rpm. Cultures were collected by centrifugation and the pellets were washed once with chilled PBS before flash-freezing with liquid nitrogen and storage at −80 °C. Functional bacterial TIR–STING constructs were expressed in cultures additionally supplemented with 10–30 mM nicotinamide to limit TIR toxicity.

Bacterial pellets were lysed by sonication in 1× lysis buffer (20 mM HEPES–KOH pH 7.5, 400 mM NaCl, 30 mM imidazole, 10% glycerol and 1 mM DTT). Clarified lysates were purified by gravity-flow over Ni-NTA resin (Qiagen). Resin was washed with 1× lysis buffer supplemented to 1 M NaCl, and recombinant protein was eluted with 1× lysis buffer supplemented to 300 mM imidazole. Recombinant human SENP2 protease (D364–L589, M497A) was incubated with purified samples overnight during dialysis at 4 °C against dialysis buffer (20 mM HEPES–KOH pH 7.5, 250 mM KCl, 10% glycerol, 1 mM DTT) to cleave the SUMO2 tag. Proteins were concentrated with 30-kDa-cutoff Amicon centrifuge filters (Millipore) before loading onto a 16/600 Superdex 200 size-exclusion column equilibrated in gel filtration buffer (20 mM HEPES–KOH pH 7.5, 250 mM KCl, 1 mM TCEP). Protein purity was assessed by SDS–PAGE with Coomassie staining before concentrating samples to >10 mg ml^{-1}. Final proteins samples were flash-frozen in liquid nitrogen and stored at −80 °C.

Synthetic cyclic dinucleotide standards

Synthetic cyclic dinucleotide ligands used for structural biology and biochemistry experiments were purchased from Biolog Life Science Institute: 3′,3′-c-di-AMP (cat no. C 088), 3′,3′-c-di-GMP (cat no. C 057), 3′,3′-cGAMP (cat no. C 117), 2′,3′-cGAMP (cat no. C 161), 3′,3′-c-UMP–AMP (cat no. C 357) and 2′,3′-c-di-GMP (cat no. C 182).

Protein crystallization and structure determination

Crystals for all proteins were initially grown at 18 °C using the hanging-drop vapour diffusion method. Concentrated protein stocks were thawed from −80 °C on ice and diluted in buffer (25 mM HEPES–KOH pH 7.5, 70 mM KCl, 1 mM TCEP) to final concentration. STING–cyclic dinucleotide complexes were formed by incubating protein with ligand on ice for 20 min before setting trays. In all cases, optimized crystals were obtained using EasyXtal 15-well hanging-drop trays (Qiagen) in 2-μl drops mixed 1:1 over a 350-μl reservoir of mother liquor after 1–3 d of growth at 18 °C. Final optimized crystal-growth conditions were as follows: crystals of native and selenomethionine-substituted FsSTING bound to 3′,3′-cGAMP grew at 10 mg ml^{-1} with 0.5 mM 3′,3′-cGAMP in 2 M ammonium sulfate, 0.2 M sodium acetate pH 4.5 and were cryoprotected with NVH oil (Hampton). Crystals of selenomethionine-substituted *Cg*STING grew at 18 mg ml^{-1} with 0.5 mM c-di-GMP in 0.1 M HEPES–NaOH pH 7.5, 20% PEG-10,000 and were cryoprotected with mother liquor supplemented with 20% ethylene glycol (*Cg*STING continually precipitated upon incubation with c-di-GMP probably resulting in specific crystallization of the soluble apo form). Crystals of selenomethionine-substituted FsCdnE grew at 7 mg ml^{-1} with 10.5 mM $MgCl_2$ and 0.5 mM GpCpp in 0.1 M sodium acetate pH 4.6, 2 M sodium formate and were cryoprotected by supplementing reservoir solution with 25% ethylene glycol and 0.5 mM GpCpp. Crystals of selenomethionine-incorporated *Cg*CdnE grew at 7 mg ml^{-1} with 10.5 mM $MgCl_2$ and 0.5 mM GpCpp and grew in 0.2 M sodium thiocyanate, 20% PEG-3350 and were cryoprotected with NVH oil (Hampton). No GpCpp density is visible in either of the FsCdnE or *Cg*CdnE crystal structures. Crystals of apo oyster TIR–STING (*C. gigas* XP_011430837.1) grew at 7 mg ml^{-1} in 0.2 M $MgCl_2$, 0.1 M Tris pH 8.5, and 16% PEG-4000 and were cryoprotected by supplementing mother liquor with 20% glycerol. Crystals of oyster TIR–STING bound to 2′,3′-cGAMP grew at 7 mg ml^{-1} protein with 0.5 mM 2′,3′-cGAMP in 0.2 M ammonium citrate pH 7.0, 20% PEG-3350 and were cryoprotected with mother liquor supplemented with 20% ethylene glycol and 0.5 mM 2′,3′-cGAMP. X-ray diffraction data were collected with single crystals at the Advanced Photon Source (beamlines 24-ID-C and 24-ID-E) with a wavelength of 0.97918 Å and temperature of 80 K.

Data were processed with XDS and AIMLESS[38] using the SSRL autoxds script (A. Gonzalez). Experimental phase information for all proteins was determined using data collected from selenomethionine-substituted crystals. Anomalous sites were identified and an initial map generated with AutoSol within PHENIX 1.17[39]. Iterative model building and refinement was performed using Coot 0.8.9[40] and PHENIX. Final structures were refined to stereochemistry statistics for Ramachandran plot, rotamer outliers and MolProbity score as follows: FsSTING–3′,3′-cGAMP, 97.49%/2.51% (favoured/allowed), 1.12% and 1.26; *Cg*STING apo, 97.23%/2.77%, 1.90% and 1.55; *C. gigas* STING apo, 95.68%/4.32%, 0.72% and 1.58; *C. gigas* STING–2′,3′-cGAMP, 97.25%/2.75%, 0.67% and 1.38; FsCdnE apo, 98.86%/1.14%, 0.30% and 0.97; *Cg*CdnE, 98.63%/1.37%, 0.70% and 1.09. Deposited PDB codes are in Supplementary Table 1 and 'Data availability'. All structure figures were generated with PyMOL 2.3.4.

Structure-guided alignment of bacterial and metazoan STING domains

To guide alignment and phylogenetic analysis of all STING family receptors, the bacterial FsSTING, *Cg*STING and oyster STING structures were superposed with human STING and representatives from all previously published metazoan STING structures[6–9,12,19,23,41–47] using the secondary-structure matching algorithm in Coot[40,48]. A sequence alignment was extracted from the superposed structures according to Cα position, and extended to include a list of all known STING protein sequences using PROMALS3D[49]. In brief, the list of bacterial STING protein sequences was prepared from analysis of bacterial defence islands as described in 'Phylogenetic distribution of STING-domain proteins in bacterial genomes' and included 103 sequences. Sequences were aligned with MAFFT[50] and manually trimmed in Jalview[51] based on boundaries of the FsSTING crystal structure to remove effector domain sequences and obtain an alignment of the STING

cyclic-dinucleotide-binding domain. Metazoan STING sequences were obtained from the Interpro (IPR033952) and Pfam (PF15009) databases and trimmed to the cyclic-dinucleotide-binding domain based on boundaries of the human STING and oyster STING crystal structures, resulting in 492 unique sequences. The output PROMALS3D alignment was inspected to ensure accurate secondary-structure matching between bacterial and metazoan STING, and includes 34 gap-free sites. A STING family phylogenetic tree was then calculated using the MAFFT server and visualized with iTOL[52] for analysis.

Cyclic dinucleotide synthesis and thin-layer chromatography analysis

CdnE homologues were tested for cyclic dinucleotide synthesis capability using α^{32}P-labelled NTPs and product resolution with thin-layer chromatography as previously described[15]. In a 20-µl final reaction volume, 5 µM enzyme was incubated with 25 µM of each cold NTP (ATP, GTP, CTP and UTP, 100 µM total) and with trace radiolabelled NTP (about 1 µCi) as indicated for 3 h at 37 °C in buffer containing 50 mM Tris-HCl pH 7.5, 50 mM KCl, 10 mM magnesium acetate, and 1 mM TCEP. Reactions were treated with calf intestinal phosphatase (New England Biolabs) at 37 °C for 30 min to remove excess starting nucleotides. Then, 0.5 µl of sample was separated on a PEI-Cellulose F TLC plate (EMD Biosciences) using a running solvent of 1.5 M KH_2PO_4 pH 3.8 for 0.5–1 h. Plates were dried for 1 h at ambient temperature before exposure to a phosphor-screen and imaging with a Typhoon Trio Variable Mode Imager (GE Healthcare). Control cyclic dinucleotides were generated with recombinant purified *Mus musculus* cGAS, *Vibrio cholerae* DncV, *Bacillus thuringiensis* DisA, *E. coli* CdnE and *P. aeruginosa* WspR (with D70E constitutively activating mutation) as previously described[15,53]. cGAS reactions were additionally supplemented with 5 µM ISD45 double-stranded DNA for enzyme activation[37]. *E. coli* CdnE reactions to generate 3′,3′-c-UMP–AMP were conducted at pH 9.4 with 50 mM CAPSO.

STING–cyclic dinucleotide complex formation and electrophoretic mobility shift assay

STING interactions with cyclic dinucleotide ligands were monitored by electrophoretic mobility shift assay, as previously described[8]. Each 10 µl reaction was generated in buffer (5 mM magnesium acetate, 50 mM Tris-HCl pH 7.5, 50 mM KCl, and 1 mM TCEP) with 20 µM final protein concentration and 1 µM α^{32}P-labelled cyclic dinucleotide (about 0.1 µCi). Protein titration reactions used serial dilutions of stock protein to final concentrations ranging from 0.3 nM to 150 µM, with around 250 nM cyclic dinucleotide. Reactions were incubated at 25 °C for 5 min before resolution on a 7.2-cm 6% nondenaturing polyacrylamide gel run at 100 V for 45 min in 0.5× TBE buffer. The gel was fixed for 15 min in a solution of 40% ethanol and 10% acetic acid before drying at 80 °C for 1 h. The dried gel was exposed to a phosphor-screen and imaged on a Typhoon Trio Variable Mode Imager (GE Healthcare). Signal intensity was quantified using ImageQuant 5.2 software.

TIR NAD^+ cleavage activity analysis with fluorescent ε-NAD

Plate reader reactions were prepared in a 96-well plate format in 50-µl final volume with reaction buffer (20 mM HEPES–KOH pH 7.5, 100 mM KCl), 500 µM ε-NAD, 500 nM protein and between 1 nM–100 µM cyclic dinucleotide, as indicated. In brief, a master mix was prepared on ice containing each ligand and protein was added immediately before beginning analysis. Reactions were read in 96-well plates continuously over 1 h using a Synergy H1 Hybrid Multi-Mode Reader (BioTek) in fluorescence mode at 410 nm after excitation at 300 nm. Reactions were performed in technical duplicate and data are representative of independent biological replicates. Error bars indicate standard error of the mean for biological replicates. TIR oligomerization dependence experiments were performed in the absence of cyclic dinucleotide using glutathione or nickel-NTA resin at a 1:1 ratio, as previously described[21,22]. Resin was pre-equilibrated and re-suspended in 100 µl of buffer containing 500 nM protein, 20 mM HEPES–KOH pH 7.5, 100 mM KCl and 500 µM ε-NAD, and 50 µl of mixture was used for analysis.

High-performance liquid chromatography TIR NAD^+ cleavage activity analysis

High-performance liquid chromatography (HPLC) was used to measure TIR–STING NAD^+ cleavage activity and to directly observe product formation. Reactions were prepared in 20 mM HEPES–KOH pH 7.5, 100 mM KCl at a final concentration of 500 nM enzyme with or without addition of 10 µM of cyclic dinucleotides, or as indicated. TIR–STING and cyclic dinucleotide ligands were incubated on ice for 10 min before addition of NAD^+ at 500 µM. Reactions were incubated for 1 h at 25 °C, and then heat-inactivated at 95 °C for 1 min and incubation on ice for at least 5 min. Reactions were filtered through Millipore Amicon Ultra 0.5-ml filters with a 30-kDa cutoff by centrifugation for 10 min at 9,300*g* to remove protein before HPLC analysis. Products were separated and analysed by HPLC with absorbance monitoring at 254 nm. Samples were injected onto a C18 column (Zorbax Bonus-RP 4.6 × 150 mm, 3.5 µm) attached to an Agilent 1200 Infinity Series LC system. Two separate elution strategies were used: (1) isocratic elution at 40 °C with a flow rate of 1 ml min^{-1} with 50 mM NaH_2PO_4 pH 6.8 supplemented with 3% acetonitrile; and (2) gradient elution at 50 °C with a flow rate of 1 ml min^{-1} using solvent A (10 mM ammonium acetate) and solvent B (100% methanol), and a gradient from 5–100% solvent B over 12 min.

Reactions to measure discontinuous kinetics were assembled on ice in reaction buffer (20 mM HEPES–KOH pH 7.5, 100 mM KCl) with final concentration of 50 nM protein, 2 µM c-di-GMP and indicated concentrations of NAD^+. Reactions were started simultaneously and quenched after 10, 30, 120, 300 and 600 s. Products were analysed by HPLC as described in the previous paragraph, product ADPr peaks were integrated for each time point and concentrations were calculated according to a standard curve. Data were analysed using GraphPad Prism 8.4.2 software and the kinetics data fitted using a Michaelis–Menten model to calculate K_m and V_{max}. Results are representative of two independent biological replicates and plotted with errors bars denoting the standard deviation.

STING toxicity analysis in *E. coli*

*Sf*STING and mutant constructs were cloned into pBAD33 for arabinose-inducible expression in *E. coli* strain MG1655. Cells were transformed by electroporation, four colonies for each construct were sequence-verified and used to inoculate individual LB liquid cultures supplemented with 30 µg ml^{-1} chloramphenicol for 6 h at 37 °C with 200 rpm shaking. Cultures were diluted 1:10 into fresh LB medium with 30 µg ml^{-1} chloramphenicol, and 180 µl of diluted culture was divided into wells in a 96-well plate. Plate cultures were supplemented with 0.2% arabinose and 30 mM nicotinamide, as indicated, to a final volume of 200 µl per well. The OD_{600} was followed using a TECAN Infinite 200 plate reader with measurement every 10 min.

Electron microscopy sample preparation, data collection and processing

Samples for negative-stain electron microscopy analysis were prepared by diluting purified *Sf*STING (E84A mutation) protein alone, or with an equimolar-ratio cyclic dinucleotide as indicated, to a concentration of 50 µM in gel filtration buffer (20 mM HEPES–KOH pH 7.5, 150 mM KCl, 1 mM TCEP). Protein samples were further serially diluted in gel filtration buffer to a final concentration of 0.026 mg ml^{-1}. For protein–ligand mixtures, gel filtration buffer was supplemented with 1 µM of ligand for each serial dilution step. Three µl of the diluted sample was applied onto a glow-discharged (30 s, 30 mA) 400-mesh copper grid (Electron Microscopy Sciences) coated with an approximately 10-nm layer of continuous carbon (Safematic CCU-010), followed by a 30-s absorption step and side blotting to remove bulk solution. The grid was immediately stained with 1.5% uranyl formate and then blotted

from the side. The staining procedure was repeated twice with a 30-s incubation with uranyl formate before the final blotting step. The grid was air-dried before imaging.

Electron microscopy images for 2D classification were collected using an FEI Tecnai T12 transmission electron microscope operating at 120 keV and equipped with a Gatan 4,000 × 4,000 charge-coupled device (CCD) camera at a nominal magnification of 67,000×, pixel size of 1.68 Å, at a nominal defocus range of 1.0–2.0 µm. Electron microscopy images for *Sf*STING oligomerization mutants (R307E, A309R; L201R, D203R; Δ L275–Q282) were collected using a Philips CM10 transmission electron microscope operating at 100 keV and equipped with a Gatan UltraScan 894 (2,000 × 2,000) CCD camera at a nominal magnification of 52,000×, pixel size of 2.06 Å, at a nominal defocus range of 1.5 µm.

Micrographs were converted to JPEG format using e2proc2d.py script[54]. All image processing was performed in RELION-3[55]. After CTF estimation with GCTF[56], particle picking was carried out with gautomatch (K. Zhang, https://www.mrc-lmb.cam.ac.uk/kzhang/) followed by manual review. Where present, fibres were picked separately and treated as independent datasets. Particles were extracted with a 224-pixel box size (about 375 Å) and subjected to one round of 2D reference-free classification to generate 2D class averages.

Size-exclusion chromatography with multi-angle light scattering

Purified protein samples for size-exclusion chromatography with multi-angle light scattering (SEC-MALS) analysis were diluted in ice-cold running buffer (150 mM KCl, 20 mM HEPES–KOH pH 7.5, and 1 mM TCEP) to a final concentration of 2 mg ml^{-1}. Samples including ligand were prepared with 100 µM cyclic dinucleotide and incubated on ice for at least 5 min. All samples were subjected to brief centrifugation (21,000*g*, 5 min, 4 °C) to remove precipitated protein before injection onto an SRT SEC-300 column (SEPAX). Refractive index (dRI) was measured with a Wyatt Optilab T-rex Refractive Index Detector and protein concentration estimated assuming a dn/dc of 0.185. The system was also equipped with a Wyatt Dawn Heleos II Multi-Angle Light Scattering detector used to determine molar mass. All analysis was carried out using ASTRA 7 software and figures produced with GraphPad Prism 8.4.2.

Reporting summary

Further information on research design is available in the Nature Research Reporting Summary linked to this paper.

Data availability

Data that support the findings of this study are available within the Article, its Extended Data and Supplementary Information. IMG database accessions are listed in Extended Data Fig. 1, and PDB accessions are listed in each figure legend. Coordinates and structure factors of FsSTING–3′,3′-cGAMP, *Cg*STING, oyster TIR–STING, oyster TIR–STING–2′,3′-cGAMP, FsCdnE and *Cg*CdnE have been deposited in PDB under accession codes 6WT4, 6WT5, 6WT6, 6WT7, 6WT8 and 6WT9, respectively. Source data are provided with this paper.

35. Millman, A., Melamed, S., Amitai, G. & Sorek, R. Diversity and classification of cyclic-oligonucleotide-based anti-phage signalling systems. *Nat. Microbiol*. https://doi.org/10.1038/s41564-020-0777-y (2020).
36. Chen, I. A. et al. IMG/M v.5.0: an integrated data management and comparative analysis system for microbial genomes and microbiomes. *Nucleic Acids Res*. **47**, D666–D677 (2019).
37. Zhou, W. et al. Structure of the human cGAS–DNA complex reveals enhanced control of immune surveillance. *Cell* **174**, 300–311 (2018).
38. Kabsch, W. Xds. *Acta Crystallogr. D* **66**, 125–132 (2010).
39. Adams, P. D. et al. PHENIX: a comprehensive Python-based system for macromolecular structure solution. *Acta Crystallogr. D* **66**, 213–221 (2010).
40. Emsley, P. & Cowtan, K. Coot: model-building tools for molecular graphics. *Acta Crystallogr. D* **60**, 2126–2132 (2004).
41. Huang, Y. H., Liu, X. Y., Du, X. X., Jiang, Z. F. & Su, X. D. The structural basis for the sensing and binding of cyclic di-GMP by STING. *Nat. Struct. Mol. Biol*. **19**, 728–730 (2012).
42. Shang, G. et al. Crystal structures of STING protein reveal basis for recognition of cyclic di-GMP. *Nat. Struct. Mol. Biol*. **19**, 725–727 (2012).
43. Shu, C., Yi, G., Watts, T., Kao, C. C. & Li, P. Structure of STING bound to cyclic di-GMP reveals the mechanism of cyclic dinucleotide recognition by the immune system. *Nat. Struct. Mol. Biol*. **19**, 722–724 (2012).
44. Yin, Q. et al. Cyclic di-GMP sensing via the innate immune signaling protein STING. *Mol. Cell* **46**, 735–745 (2012).
45. Cavlar, T., Deimling, T., Ablasser, A., Hopfner, K. P. & Hornung, V. Species-specific detection of the antiviral small-molecule compound CMA by STING. *EMBO J*. **32**, 1440–1450 (2013).
46. Zhang, H. et al. Rat and human STINGs profile similarly towards anticancer/antiviral compounds. *Sci. Rep*. **5**, 18035 (2015).
47. Cong, X. et al. Crystal structures of porcine STING^{CBD}–CDN complexes reveal the mechanism of ligand recognition and discrimination of STING proteins. *J. Biol. Chem*. **294**, 11420–11432 (2019).
48. Krissinel, E. & Henrick, K. Secondary-structure matching (SSM), a new tool for fast protein structure alignment in three dimensions. *Acta Crystallogr. D* **60**, 2256–2268 (2004).
49. Pei, J. & Grishin, N. V. PROMALS3D: multiple protein sequence alignment enhanced with evolutionary and three-dimensional structural information. *Methods Mol. Biol*. **1079**, 263–271 (2014).
50. Katoh, K., Rozewicki, J. & Yamada, K. D. MAFFT online service: multiple sequence alignment, interactive sequence choice and visualization. *Brief. Bioinform*. **20**, 1160–1166 (2019).
51. Waterhouse, A. M., Procter, J. B., Martin, D. M., Clamp, M. & Barton, G. J. Jalview Version 2—a multiple sequence alignment editor and analysis workbench. *Bioinformatics* **25**, 1189–1191 (2009).
52. Letunic, I. & Bork, P. Interactive Tree Of Life (iTOL) v4: recent updates and new developments. *Nucleic Acids Res*. **47**, W256–W259 (2019).
53. Kulasakara, H. et al. Analysis of *Pseudomonas aeruginosa* diguanylate cyclases and phosphodiesterases reveals a role for bis-(3′-5′)-cyclic-GMP in virulence. *Proc. Natl Acad. Sci. USA* **103**, 2839–2844 (2006).
54. Tang, G. et al. EMAN2: an extensible image processing suite for electron microscopy. *J. Struct. Biol*. **157**, 38–46 (2007).
55. Zivanov, J. et al. New tools for automated high-resolution cryo-EM structure determination in RELION-3. *eLife* **7**, e42166 (2018).
56. Zhang, K. Gctf: real-time CTF determination and correction. *J. Struct. Biol*. **193**, 1–12 (2016).
57. Kranzusch, P. J. et al. Structure-guided reprogramming of human cGAS dinucleotide linkage specificity. *Cell* **158**, 1011–1021 (2014).

Acknowledgements We thank J. Morehouse, A. Lee, K. Chat, R. Vance and members of the Kranzusch laboratory for helpful comments and discussion; K. Arnett and the Harvard University Center for Macromolecular Interactions; the Molecular Electron Microscopy Suite at Harvard Medical School; and the Harvard Center for Mass Spectrometry. The work was funded by the Richard and Susan Smith Family Foundation (P.J.K. and S.S.), DFCI-Novartis Drug Discovery Program (P.J.K.), the Parker Institute for Cancer Immunotherapy (P.J.K.), a Cancer Research Institute CLIP Grant (P.J.K.), a V Foundation V Scholar Award (P.J.K.), the Pew Biomedical Scholars program (P.J.K.), Vallee Foundation (S.S.), the Ariane de Rothschild Women Doctoral Program (A.M.), the Israeli Council for Higher Education via the Weizmann Data Science Research Center (A.M.), the European Research Council (grant ERC-CoG 681203 to R.S.), the Ernest and Bonnie Beutler Research Program of Excellence in Genomic Medicine (R.S.), the Minerva Foundation (R.S.) and the Knell Family Center for Microbiology (R.S.). B.R.M. is supported as a Ruth L. Kirschstein NRSA Postdoctoral Fellow NIH F32GM133063, A.A.G. is supported by a United States National Science Foundation Graduate Research Fellowship, B.L. is supported as a Herchel Smith Graduate Research Fellow, G.O. is supported by a Weizmann Sustainability and Energy Research Initiative (SAERI) doctoral fellowship. X-ray data were collected at the Northeastern Collaborative Access Team beamlines 24-ID-C and 24-ID-E (P30 GM124165), and used a Pilatus detector (S10RR029205), an Eiger detector (S10OD021527) and the Argonne National Laboratory Advanced Photon Source (DE-AC02-06CH11357).

Author contributions Experiments were designed and conceived by B.R.M., R.S. and P.J.K. Structural and biochemical experiments were performed by B.R.M. with assistance from A.A.G. and P.J.K. NAD^+ cleavage assays were performed by A.A.G. and B.R.M. Gene identification and phylogenetic analysis were performed by A.M. and R.S. Electron microscopy experiments and analysis were conducted by A.F.A.K. and S.S. STING oligomerization analysis was performed by B.L. and B.R.M. STING toxicity analysis was performed by G.O. and R.S. The manuscript was written by B.R.M. and P.J.K. All authors contributed to editing the manuscript, and support the conclusions.

Competing interests The authors declare no competing interests.

Additional information

Supplementary information is available for this paper at https://doi.org/10.1038/s41586-020-2719-5.

Correspondence and requests for materials should be addressed to P.J.K.

Peer review information *Nature* thanks Urs Jenal and the other, anonymous, reviewer(s) for their contribution to the peer review of this work. Peer reviewer reports are available.

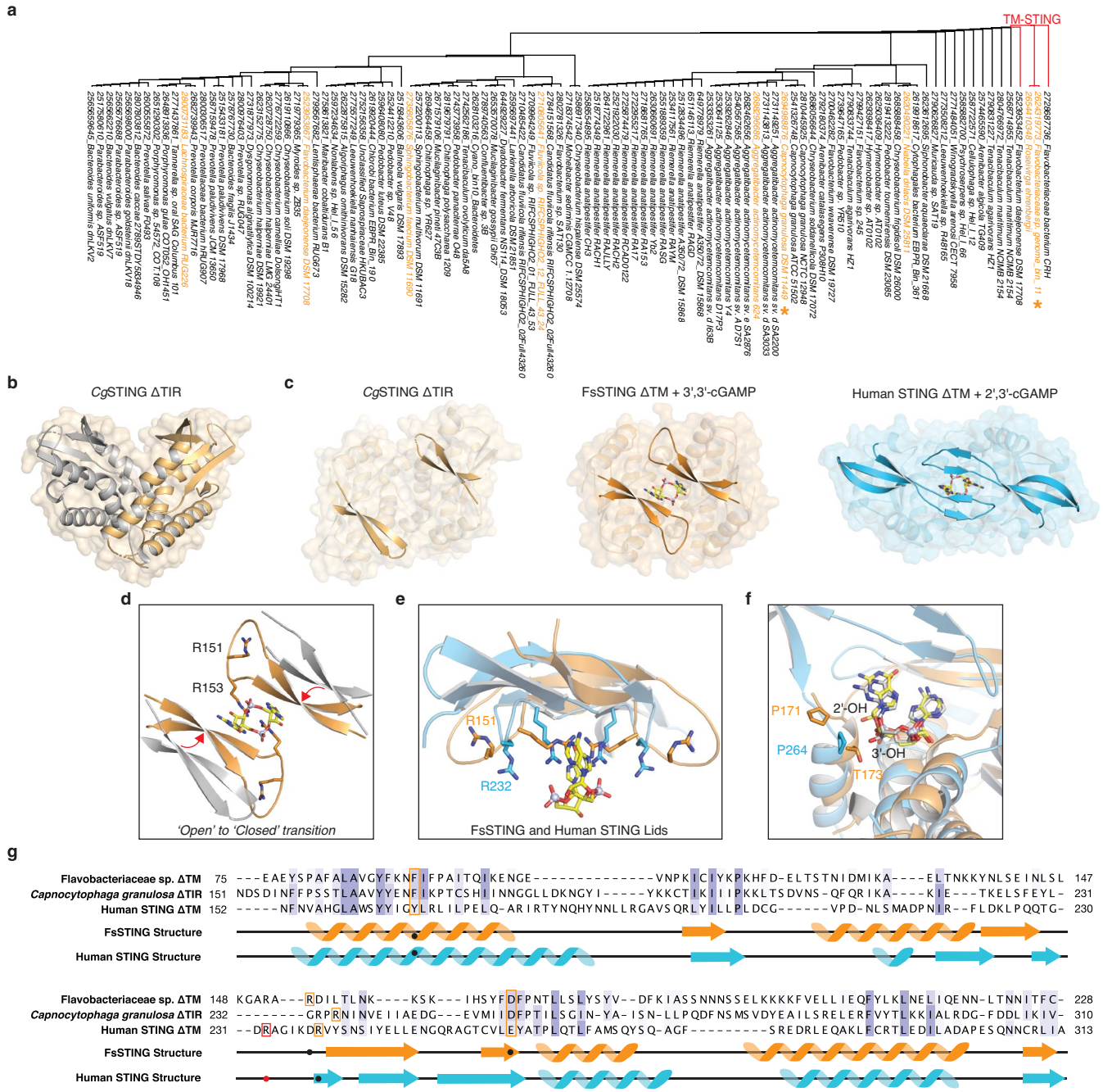

Extended Data Fig. 1 | See next page for caption.

Extended Data Fig. 1 | Structural analysis of bacterial STING–cyclic dinucleotide complex formation. a, Phylogenetic tree of all CBASS-associated bacterial STING homologues based on structure-guided sequence alignment and previous bioinformatics analysis[10,35]. STING homologues investigated in this study are highlighted in orange, and a star denotes determined STING crystal structures. All TM–STING fusions cluster together. **b**, Crystal structure of a STING receptor from the bacterium *C. granulosa* (*Cg*STING) in the apo state reveals an open configuration with a solvent exposed cyclic-dinucleotide-binding pocket at the dimeric interface (monomers in gold and grey for clarity). The *Cg*STING structure confirms that both divergent TM–STING and TIR–STING fusions are members of the same structurally conserved family of STING receptors. **c**, Comparison of the *Cg*STING, FsSTING–3′,3′-cGAMP and human STING–2′,3′-cGAMP structures demonstrates conservation of an open-to-closed β-strand lid movement upon ligand binding. **d**, Overlay of the β-strand lid of *Cg*STING (grey) and FsSTING (orange) shows both inward translation and slight rotation resulting in a displacement of about 5 Å. R153 of FsSTING stacks between the bases of 3′,3′-cGAMP and R151 is splayed away from ligand. **e**, Comparison of the human STING and FsSTING lid region shows conserved contacts from β-strand arginine residues. Unlike in bacterial STING, human STING R232 makes an additional contact with the cyclic dinucleotide phosphodiester backbone that is critical for recognition of the 2′–5′ linkage in 2′,3′-cGAMP. A detailed comparison is in Extended Data Fig. 10b. **f**, Modelling of 2′,3′-cGAMP into the FsSTING–3′,3′-cGAMP structure demonstrates an additional feature of bacterial STING preventing recognition of 2′–5′-linked cyclic dinucleotides. Although the overall cyclic dinucleotide conformation is shared between human and bacterial STING, the α-helix ending at P264 in human STING is a half-turn longer in FsSTING (also ending in a proline) which places a conserved T173 residue in a position that occludes where the free 3′-OH of 2′,3′-cGAMP would be positioned. **g**, Structure-guided alignment of FsSTING and human STING cyclic-dinucleotide-binding domains. FsSTING and human STING exhibit no detectable sequence homology but share a conserved structural fold. Key residues involved in cyclic dinucleotide binding that are shared between bacterial and human STING are boxed in orange and human STING specific cyclic dinucleotide contacts are boxed in red. In FsSTING, D169 directly reads out the guanine base of c-di-GMP.

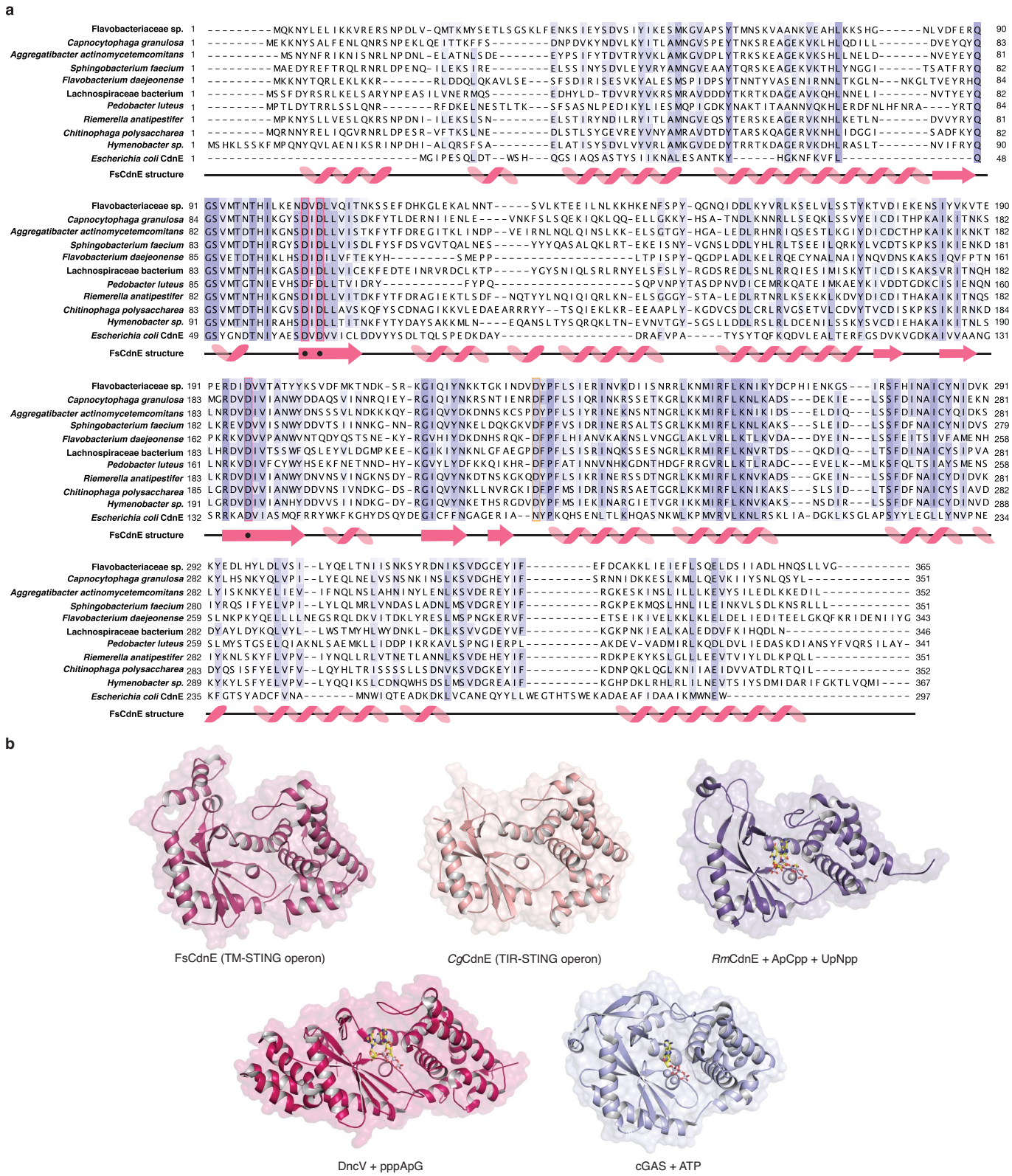

Extended Data Fig. 2 | Structural analysis of STING-associated CD-NTase enzymes. a, Sequence and secondary structure alignment of STING-associated CD-NTases reveals the extent of homology between CdnE homologues from unrelated bacterial strains. Highlighted positions include active-site residues (pink box), and an aspartic acid substitution at a position known to be involved in nucleotide substrate selection (orange box) that is unique to CD-NTases in STING-containing CBASS operons[15]. A divergent *E. coli* CdnE that synthesizes cyclic UMP–AMP is included for comparison. **b**, Crystal structures of FsCdnE and *Cg*CdnE from STING-containing CBASS operons allow direct comparison with previously determined bacterial and human CD-NTase structures. The FsCdnE and *Cg*CdnE structures are most closely related to the clade-E CD-NTase structure from *Rhodothermus marinus* CdnE (*Rm*CdnE). *Rm*CdnE: PDB 6E0L[15]; *V. cholerae* DncV: PDB 4TYO[57]; and human cGAS: PDB 6CTA (DNA omitted for clarity)[37].

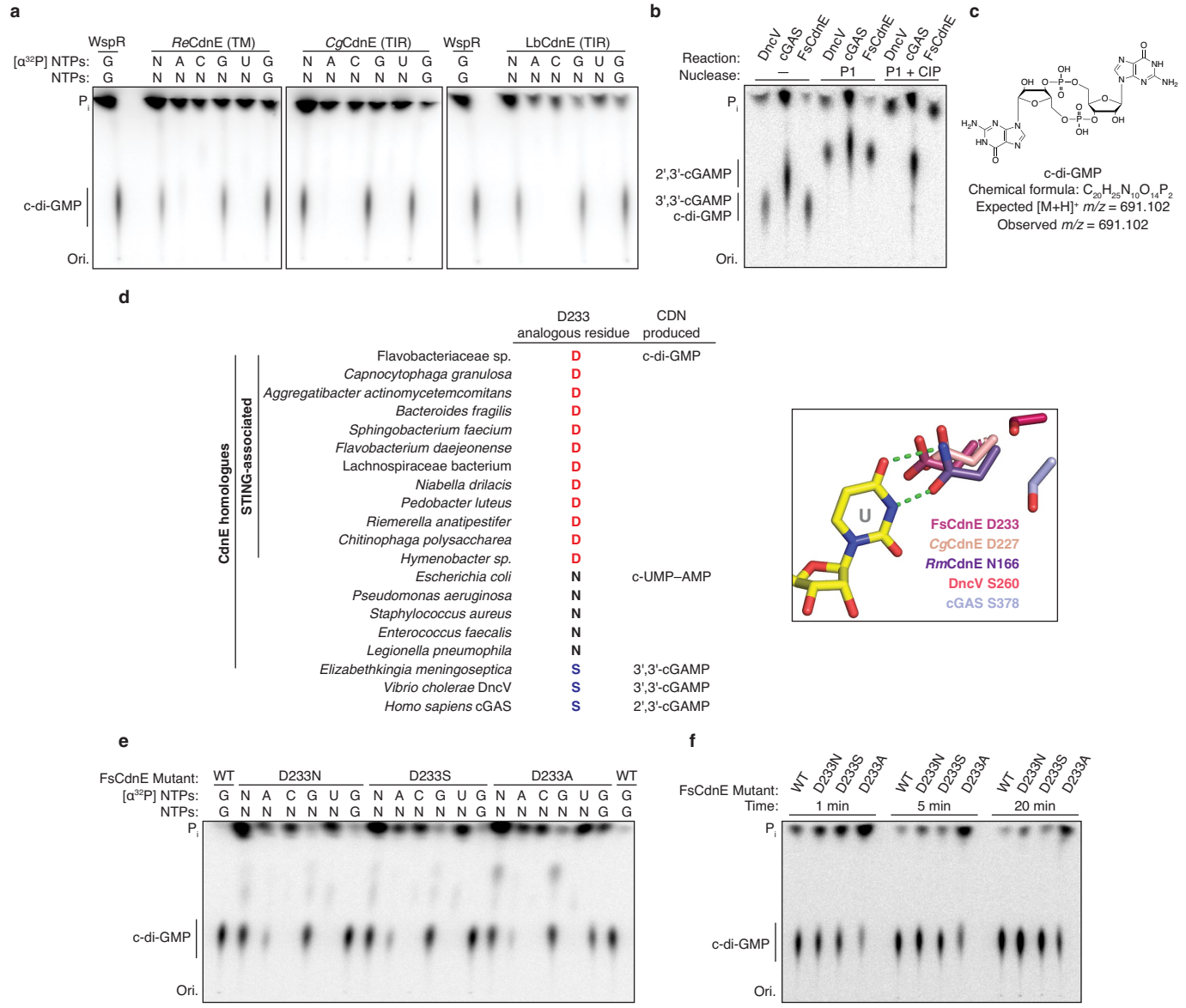

Extended Data Fig. 3 | Biochemical analysis of c-di-GMP synthesis by bacterial STING-associated CD-NTases. a, In addition to FsCdnE (Fig. 2b), CdnE homologues from three divergent STING-containing CBASS operons were purified and tested for cyclic-dinucleotide-synthesis specificity using α^{32}P-radiolabelled NTPs and thin-layer chromatography. Deconvolution experiments show a single major product requiring only GTP that migrates identically to c-di-GMP synthesized by the GGDEF enzyme WspR. All reactions were treated with alkaline phosphatase to remove exposed phosphates. Only two bacterial genomes encoding a STING-containing CBASS operon retain proteins with a predicted canonical GGDEF c-di-GMP signalling domain. The exceptions are chlorobi bacterium *EBPR_Bin_190*, which contains a single GGDEF domain that is fused to a SLATT domain and may be part of a CBASS-like system[10], and a Lachnospiraceae bacterium *RUG226* genome that encodes many GGDEF genes. The Lachnospiraceae bacterium *RUG226* CdnE retains exclusive production of c-di-GMP suggesting the CdnE–STING system is sequestered in this bacterium or that an unknown mechanism may exist to prevent toxic STING activation. *Re*CdnE, *Roseivirga ehrenbergii*; *Cg*CdnE, *Capnocytophaga granulosa*; LbCdnE, Lachnospiraceae bacterium; N, all four rNTPs; P_i, inorganic phosphate; ori., origin. Data are representative of two independent experiments. **b**, Nuclease treatment confirms that the FsCdnE enzymatic product contains only canonical 3′–5′ phosphodiester bonds. The [α^{32}P]GTP cyclic dinucleotide product is susceptible to cleavage by nuclease P1 resulting in release of GMP as a new species, which migrates further up the TLC plate. Further digestion with calf-intestinal phosphatase (CIP) removes all exposed phosphates, resulting in complete loss of a labelled product spot. DncV (Dinucleotide cyclase in *Vibrio*)-derived 3′,3′-cGAMP is similarly susceptible to complete digestion by P1 and CIP treatment, whereas 2′,3′-cGAMP synthesized by mouse cGAS is only partially digested owing to the presence of the non-canonical 2′–5′ bond. Data are representative of two independent experiments. **c**, High-resolution mass spectrometry analysis confirms the identity of the major FsCdnE enzymatic product as canonical c-di-GMP. Chemically synthesized c-di-GMP was used for direct spectral comparison. **d**, Sequence alignment and enlarged inset of the active-site of the *Rm*CdnE structure in complex with nonhydrolyzable UTP and ATP analogues (PDB 6E0L), demonstrating a contact in the CD-NTase lid domain known to control nucleobase sequence specificity[15]. *Rm*CdnE synthesizes cyclic UMP–AMP and uses N166 to specifically contact the uridine Watson–Crick edge. By contrast, FsCdnE and *Cg*CdnE contain an aspartic acid substitution at this position and synthesize c-di-GMP, and *V. cholerae* DncV and human cGAS contain a serine substitution at this position and synthesize 3′,3′-cGAMP and 2′,3′-cGAMP. An aspartic acid at the FsCdnE D233 position is conserved among 93% of STING-associated CD-NTase enzymes (96 of 103), consistent with strict specificity of c-di-GMP as the nucleotide second messenger that controls bacterial STING activation. *Rm*CdnE: PDB 6E0L[15]; *V. cholerae* DncV: PDB 4TY0[57]; and human cGAS: PDB 6CTA (DNA omitted for clarity)[37]. **e**, **f**, Mutational analysis of the importance of D233 in FsCdnE c-di-GMP synthesis activity. D233 substitutions do not disrupt the overall ability of FsCdnE to selectively synthesis c-di-GMP, but a D233A substitution causes a mild reduction in nucleobase selectivity and efficiency of c-di-GMP synthesis. These results are consistent with a role for D233 in nucleobase selection but demonstrate full selectively is achieved by additional contacts in the active site pocket. Data are representative of three independent experiments.

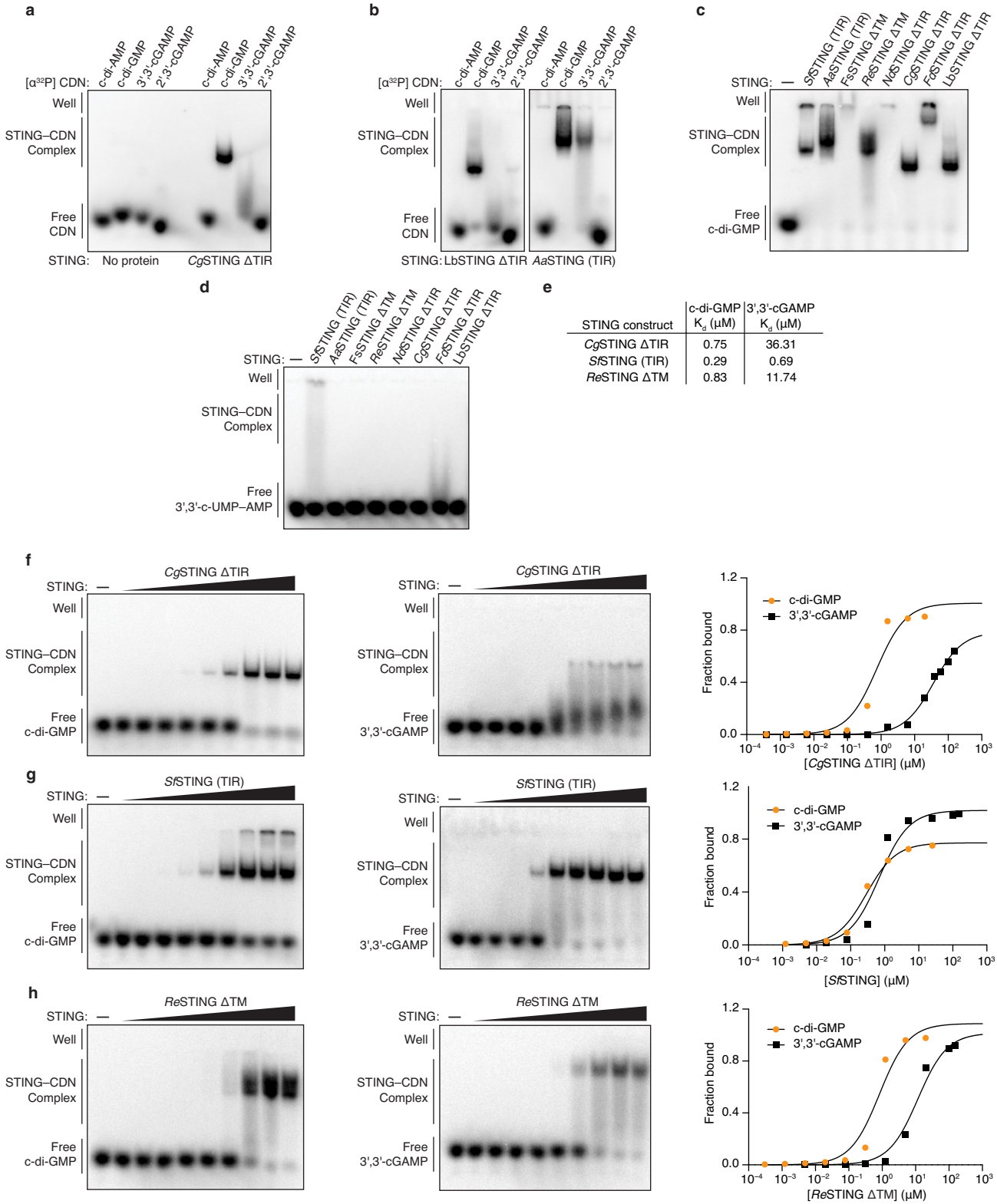

Extended Data Fig. 4 | See next page for caption.

Extended Data Fig. 4 | Biochemical analysis of bacterial STING cyclic dinucleotide recognition specificity. a, **b**, Electrophoretic mobility shift assay (EMSA) of purified bacterial STING proteins with radiolabelled cyclic dinucleotide ligands. Bacterial STING receptors specifically recognize c-di-GMP and have a weak ability to bind 3′,3′-cGAMP. No interaction was observed with c-di-AMP or 2′,3′-cGAMP. Lachnospiraceae bacterium STING: LbSTING; *Aggregatibacter actinomycetemcomitans* STING, *Aa*STING. Data are representative of two independent experiments. **c**, EMSA analysis of a diverse panel of bacterial STING homologues demonstrates conservation of c-di-GMP binding in both TM–STING and TIR–STING CBASS immunity. *Nd*STING, *Niabella drilacis*; *Fd*STING, *Flavobacterium daejeonense*. Higher-order complex formation visible as well-shifted complexes is consistent with STING oligomerization results (Fig. 3f, Extended Data Fig. 7). Data are representative of three independent experiments. **d**, EMSA analysis of diverse bacterial STING homologues broadly demonstrates no interaction with the 3′,3′-c-UMP–AMP second messenger synthesized by the divergent CD-NTase *E. coli* CdnE[15] and further confirms the specificity of c-di-GMP signalling in bacterial STING-containing CBASS operons. Data are representative of two independent experiments. **e**–**h**, EMSA analysis and quantification of the affinity of bacterial STING homologues for c-di-GMP and 3′,3′-cGAMP. Signal intensity analysis is plotted as fraction bound (shifted/total signal) as a function of increasing protein concentration and fit to a single binding isotherm. *Cg*STING and *Re*STING have a >10-fold preference for c-di-GMP whereas *Sf*STING has a similar apparent affinity for c-di-GMP and 3′,3′-cGAMP. Data are representative of two independent experiments.

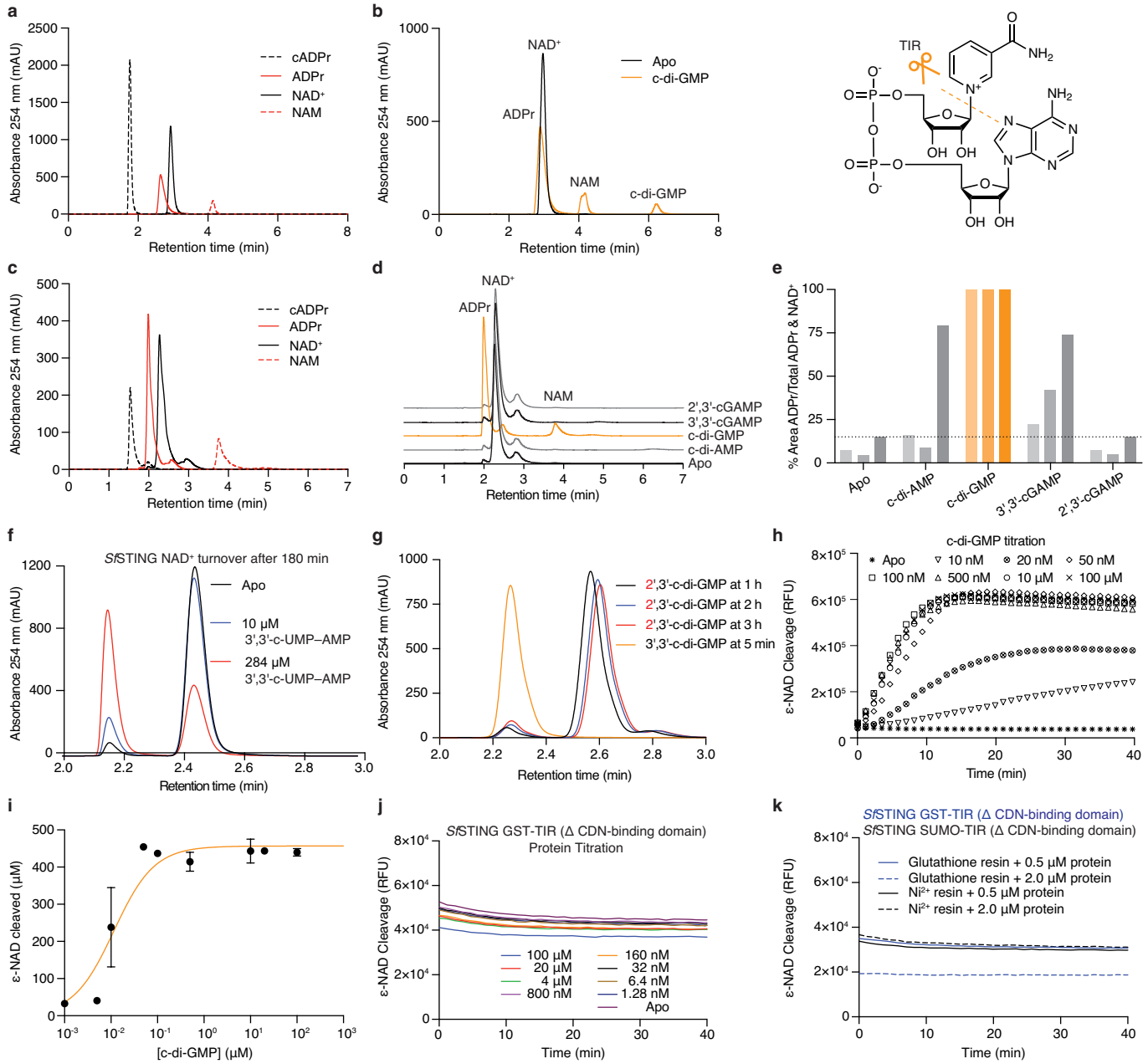

Extended Data Fig. 5 | See next page for caption.

Extended Data Fig. 5 | Bacterial STING activation of TIR NADase activity. **a**, HPLC analysis of chemical standards separated with an ammonium acetate:methanol gradient elution used to analyse bacterial TIR–STING activity (Methods). The NAD^+ and ADPr peaks have overlapping bases under these conditions. cADPr, cyclic adenosine diphosphate-ribose; ADPr, adenosine diphosphate-ribose; NAD^+, β-nicotinamide adenine dinucleotide; NAM, nicotinamide. **b**, HPLC analysis of *Sf*STING NAD^+ cleavage activity with gradient elution. *Sf*STING at 500 nM protein with 2 μM c-di-GMP converts 500 μM NAD^+ into ADPr and NAM in 30 min at ambient temperature. *Sf*STING does not generate any cyclized product and is therefore a standard glycosyl hydrolase. Inset, schematic of NAD^+ cleavage reaction. **c**, HPLC analysis of chemical standards separated with an alternative isocratic elution strategy (Methods) that results in clearer separation of NAD^+ and ADPr peaks. **d**, HPLC analysis of *Sf*STING NAD^+ cleavage activity with isocratic elution. *Sf*STING NAD^+ cleavage activity requires specific activation with c-di-GMP (30-min reactions). **e**, HPLC analysis of *Sf*STING NAD^+ cleavage activity and cyclic dinucleotide agonist specificity. Each reaction was tested with 500 nM *Sf*STING, 500 μM cyclic dinucleotide and 500 μM NAD^+ and sampled at 45, 90 or 180 min (gradient colouring in bars). *Sf*STING preferentially responds to c-di-GMP, but 3′,3′-cGAMP and c-di-AMP can function as weak agonists. Data are representative of three independent experiments. **f**, HPLC analysis of *Sf*STING NAD^+ cleavage activity in the presence of 3′,3′-c-UMP–AMP. 3′,3′-c-UMP–AMP is a >1,000×-weaker agonist than c-di-GMP. Data are representative of three independent experiments. **g**, HPLC analysis of *Sf*STING NAD^+ cleavage activity in the presence of a synthetic c-di-GMP analogue with a noncanonical 2′–5′ linkage (2′,3′-c-di-GMP). 2′,3′-c-di-GMP is not capable of stimulating robust *Sf*STING activation even at very high concentrations (250 μM versus 250 nM canonical c-di-GMP), confirming the specificity of bacterial STING for 3′–5′-linked cyclic dinucleotides. Data are representative of three independent experiments. **h**, Plate reader analysis of *Sf*STING NAD^+ cleavage activity using the fluorescent substrate ε-NAD. ε-NAD increases in fluorescence intensity after cleavage. *Sf*STING exhibits rapid catalysis with complete turnover at 500 nM protein with 500 nM c-di-GMP after 10 min at 25 °C. No background activity is observed in the absence of ligand. Data are representative of three independent experiments. **i**, Plate reader analysis of *Sf*STING NAD^+ cleavage activity in the presence of 500 nM protein with increasing c-di-GMP concentration reveals that low nM c-di-GMP levels are sufficient to induce ε-NAD cleavage. Greater c-di-GMP concentrations are required for maximal activity, consistent with binding data and the higher amount of c-di-GMP required for complete stabilization of the *Sf*STING–c-di-GMP complex (Extended Data Fig. 4e–h). Saturation occurs above 100 nM c-di-GMP with 40-min reactions. Data are ± s.d. of $n = 3$ technical replicates and are representative of 3 independent experiments. **j**, **k**, TIR-domain NAD^+ cleavage activity requires protein oligomerization. For other systems[21,22], TIR activation has been observed at very high in vitro protein concentrations or in the presence of affinity resins as an artificial oligomerization-inducing matrix[21,22]. We used a GST–TIR construct to express the *Sf*STING TIR domain in absence of the STING cyclic-dinucleotide-binding domain and observed that even at >200× the concentrations for which the full-length protein shows c-di-GMP induced activity, or in the presence of multivalent affinity resin, no NAD^+ cleavage activity occurs. These results demonstrate NAD^+ cleavage activity specifically requires STING cyclic dinucleotide recognition for activation. Data are representative of two independent experiments.

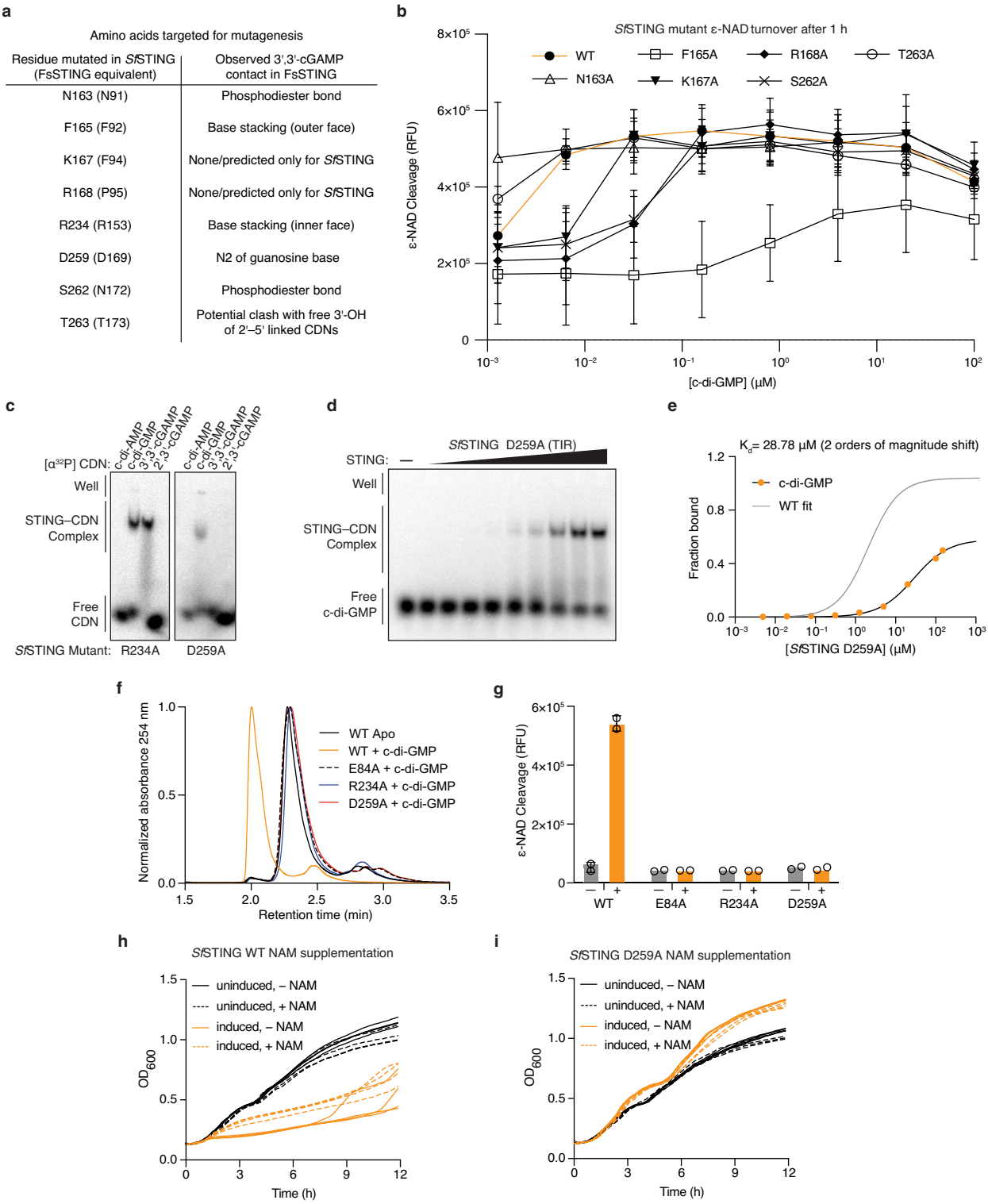

Extended Data Fig. 6 | See next page for caption.

Extended Data Fig. 6 | Mutagenesis analysis of bacterial STING cyclic dinucleotide recognition and TIR activation. a, Table of bacterial STING cyclic dinucleotide contacts tested with mutagenesis analysis. Residues were selected according to contacts observed in the structure of the FsSTING–3′,3′-cGAMP complex (FsSTING residues listed in parentheses) and tested in *Sf*STING to allow analysis of the effect on both c-di-GMP binding and NADase activity. **b**, Plate reader analysis of mutant *Sf*STING NAD^+ cleavage activity in the presence of 500 nM protein and increasing c-di-GMP concentration. Mutant *Sf*STING variants with cyclic-dinucleotide-binding pocket mutations require 10–1,000× greater c-di-GMP concentration for NADase activation. Data are ± s.d. of $n = 3$ technical replicates and are representative of 3 independent experiments. **c**–**e**, EMSA analysis demonstrating that *Sf*STING R234A and D259A mutations reduce stable c-di-GMP complex formation compared to *Sf*STING wild type (Fig. 2d). *Sf*STING(D259A) protein titration and quantification confirms significantly reduced affinity for c-di-GMP. Data are representative of three independent experiments. **f**, **g**, HPLC and plate reader analysis of mutant *Sf*STING NAD^+ cleavage activity in the presence of 500 nM protein and 10 μM c-di-GMP (HPLC) or 500 nM protein and ± 20 μM c-di-GMP (plate reader). Mutation of residues responsible for ligand recognition in the cyclic-dinucleotide-binding domain (R234 and D259) and catalysis in the TIR enzymatic domain (E84) disrupts *Sf*STING NADase activity and explains loss of *E. coli* toxicity observed in Fig. 3d. One hundred μM of c-di-GMP was used for *Sf*STING(D259A) plate reader NAD^+ cleavage analysis to confirm complete loss of c-di-GMP-induced activation. HPLC data are representative of three independent experiments. Plate reader data are ± s.d. of $n = 3$ technical replicates and are representative of 3 independent experiments. **h**, **i**, Analysis of *Sf*STING toxicity in *E. coli* cells expressing normal c-di-GMP signalling enzymes with and without nicotinamide (NAM) supplementation. NAM supplementation is sufficient to partially alleviate *Sf*STING-wild-type-induced NADase toxicity. Each line represents the average of two technical replicates for each of four separately outgrown colonies. Data are representative of two independent experiments.

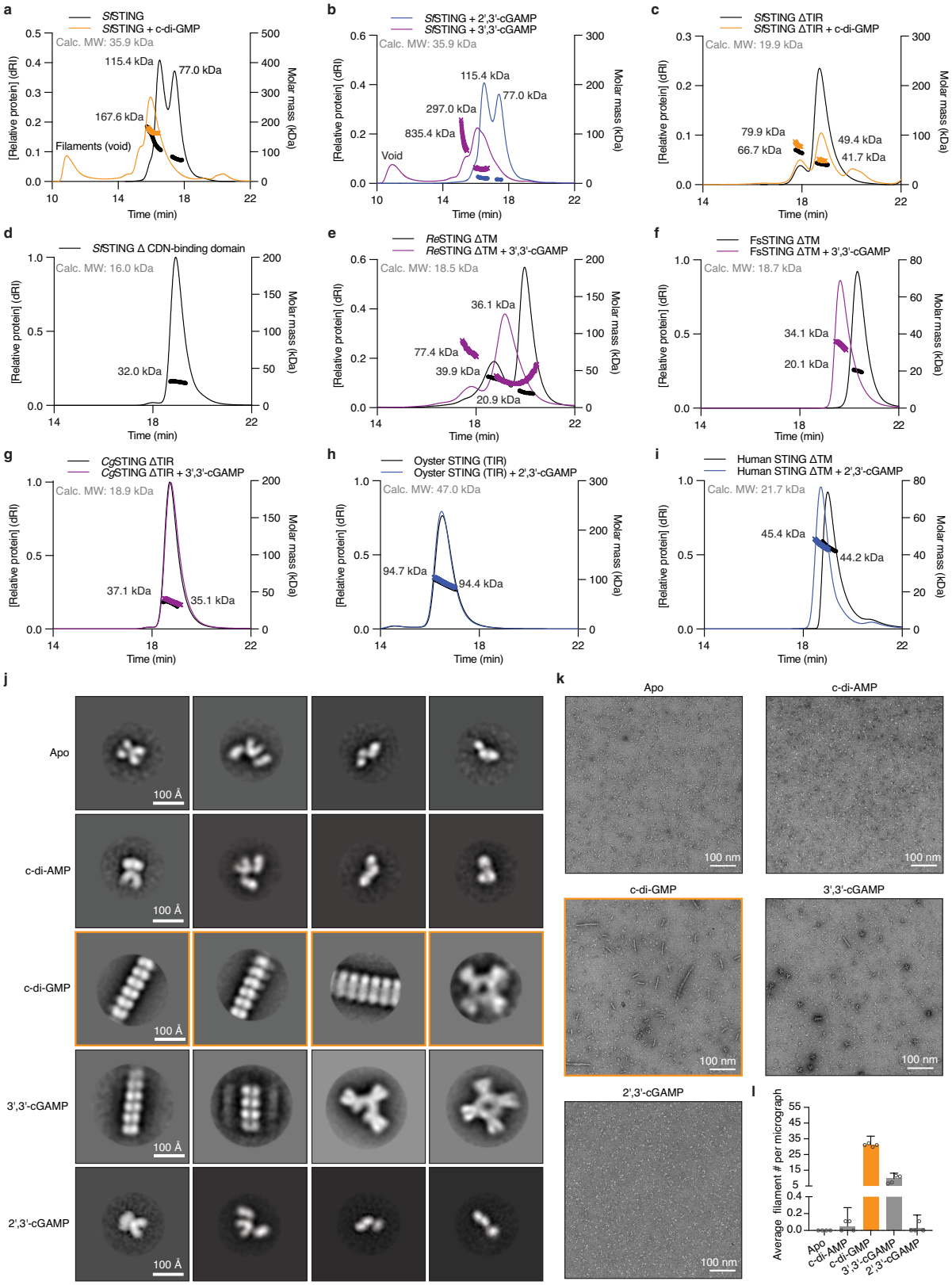

Extended Data Fig. 7 | See next page for caption.

Extended Data Fig. 7 | Conservation of oligomerization as a mechanism of STING activation. a–**i**, STING SEC-MALS analysis. **a**, **b**, Full-length *Sf*STING changes oligomeric state in the presence of c-di-GMP or the weak agonist 3′,3′-cGAMP, and does not change oligomeric state in the presence of 2′,3′-cGAMP. **c**, With the TIR domain removed (ΔTIR), *Sf*STING no longer forms higher-order complexes but notably remains dimeric in the apoprotein form. Bacterial TIR–STING proteins therefore appear to require the TIR domain to maintain stable higher-order oligomerization, suggesting that intermolecular contacts are made with both TIR and STING domains. **d**, A TIR-only construct of *Sf*STING with the cyclic-dinucleotide-binding domain removed (ΔCDN) elutes as a single species that is consistent with the molecular weight for a homodimer. **h**, Human STING (ΔTM) is a dimer in solution with or without 2′,3′-cGAMP, confirming that transmembrane contacts are required for oligomerization and filament formation[12,23]. Nearly all tested bacterial and metazoan STING constructs migrate as dimers in solution, consistent with the cyclic-dinucleotide-binding domain forming a constitutive homodimeric complex for ligand recognition. Two exceptions include *Re*STING(ΔTM) and FsSTING(ΔTM), which form a mixture of monomeric and dimeric states in the absence of ligand and dimers or tetramers in the presence of 3′,3′-cGAMP. These results indicate that alternative oligomerization events may be required for activation of bacterial TM–STING effector function. **j**, Negative-stain electron microscopy 2D class averages for *Sf*STING (E84A mutant) alone or in the presence of cyclic dinucleotide ligands. Stable STING filament formation requires c-di-GMP. Two-dimensional class averages were derived from particles selected from 75 micrographs for each condition. **k**, Representative micrograph images reveal extensive filament formation of varying length and orientation in the presence of c-di-GMP. Apo, c-di-AMP and 2′,3′-cGAMP micrographs lack filaments. Images are each representative of $n = 75$ micrographs for each condition. **l**, Particle counting analysis of micrograph images shows that c-di-GMP induces more filament formation than 3′,3′-cGAMP, and stable filament formation does not occur in the presence of c-di-AMP or 2′,3′-cGAMP. Data are mean ± s.d. for quantification of $n = 4$ groups of 10 micrograph images each.

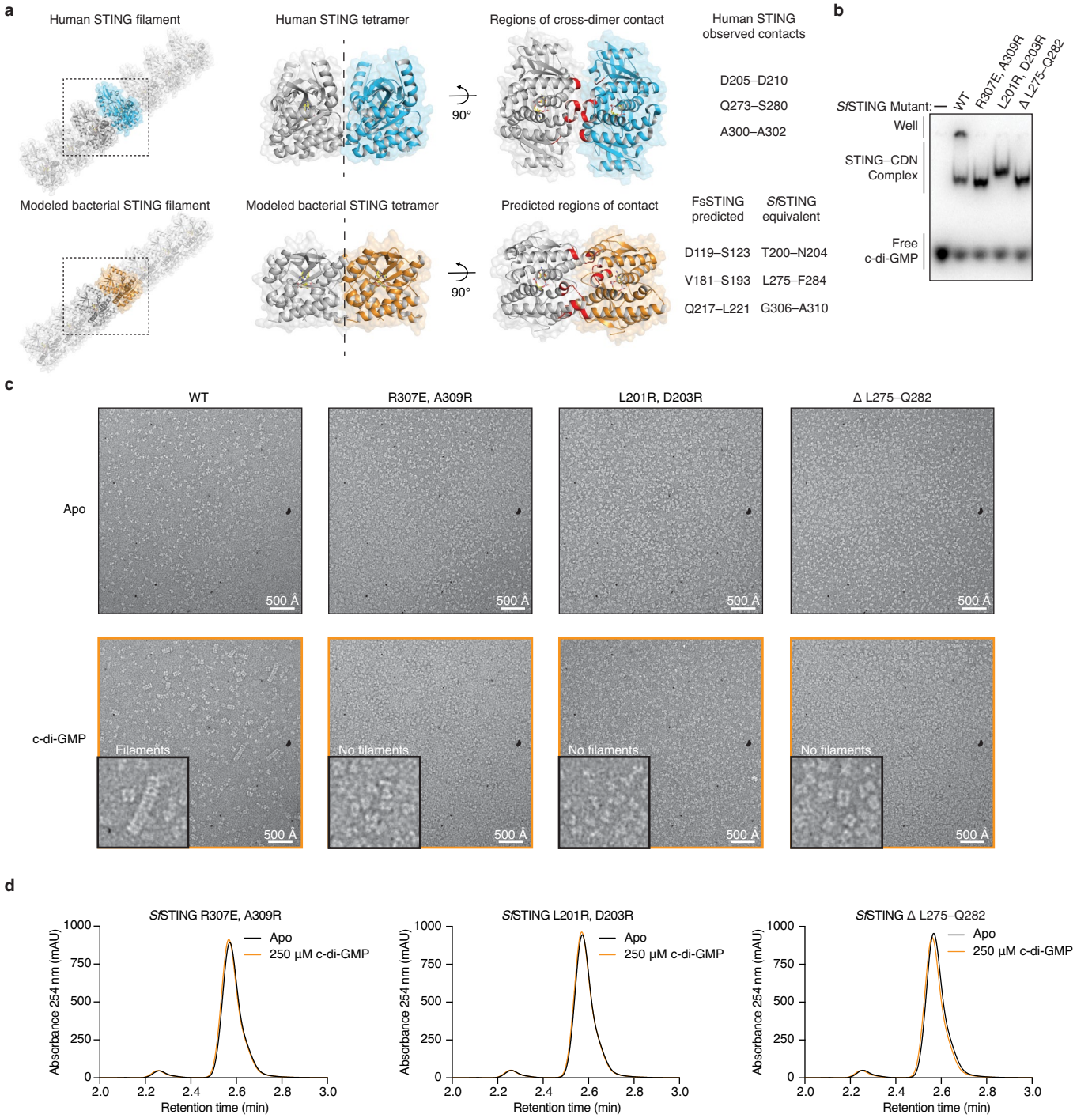

Extended Data Fig. 8 | Filament formation is required for bacterial TIR–STING activation. a, Model of bacterial STING oligomerization and identification of surfaces involved in c-di-GMP-mediated filament formation. Electron microscopy analysis of *Sf*STING in the presence of c-di-GMP reveals filament formation probably occurs through parallel stacking of the homodimeric cyclic-dinucleotide-binding domain (Extended Data Fig. 7). To construct a potential model of this interaction, we used the X-ray crystal structure of the human STING–2′,3′-cGAMP complex (PDB 4KSY)[7] and the cryo-electron microscopy structure of the chicken STING tetramer (PDB 6NT8)[9] (top) as guides to position the FsSTING–3′,3′-cGAMP complex structure into a tetrameric conformation. The resulting model predicts that oligomerization-mediating surfaces in *Sf*STING include T200–N204, L275–F284 and G306–A310. **b**, EMSA analysis of *Sf*STING variants indicates that mutations to the predicted oligomerization surfaces do not prevent c-di-GMP recognition. *Sf*STING mutants tested include R307E/A309R, L201R/D203R and the loop L275–Q282 replaced with a short GlySer linker (GSGGS). Data are representative of two independent experiments. **c**, Electron microscopy analysis of *Sf*STING variants in the presence of c-di-GMP. Mutations to the *Sf*STING surfaces identified in the structural model prevent all observable cyclic-dinucleotide-induced filament formation, supporting their predicted role in mediating oligomerization and bacterial STING filament formation. Images are each representative of $n = 5$ micrographs for each condition. **d**, HPLC analysis of mutant *Sf*STING NAD^+ cleavage activity in the presence of 500 nM protein and 250 μM c-di-GMP for 3 h. In the absence of cyclic-dinucleotide-mediated oligomerization, all *Sf*STING NADase activity is lost, confirming the requirement of filament formation in TIR domain activation. Data are representative of three independent experiments.

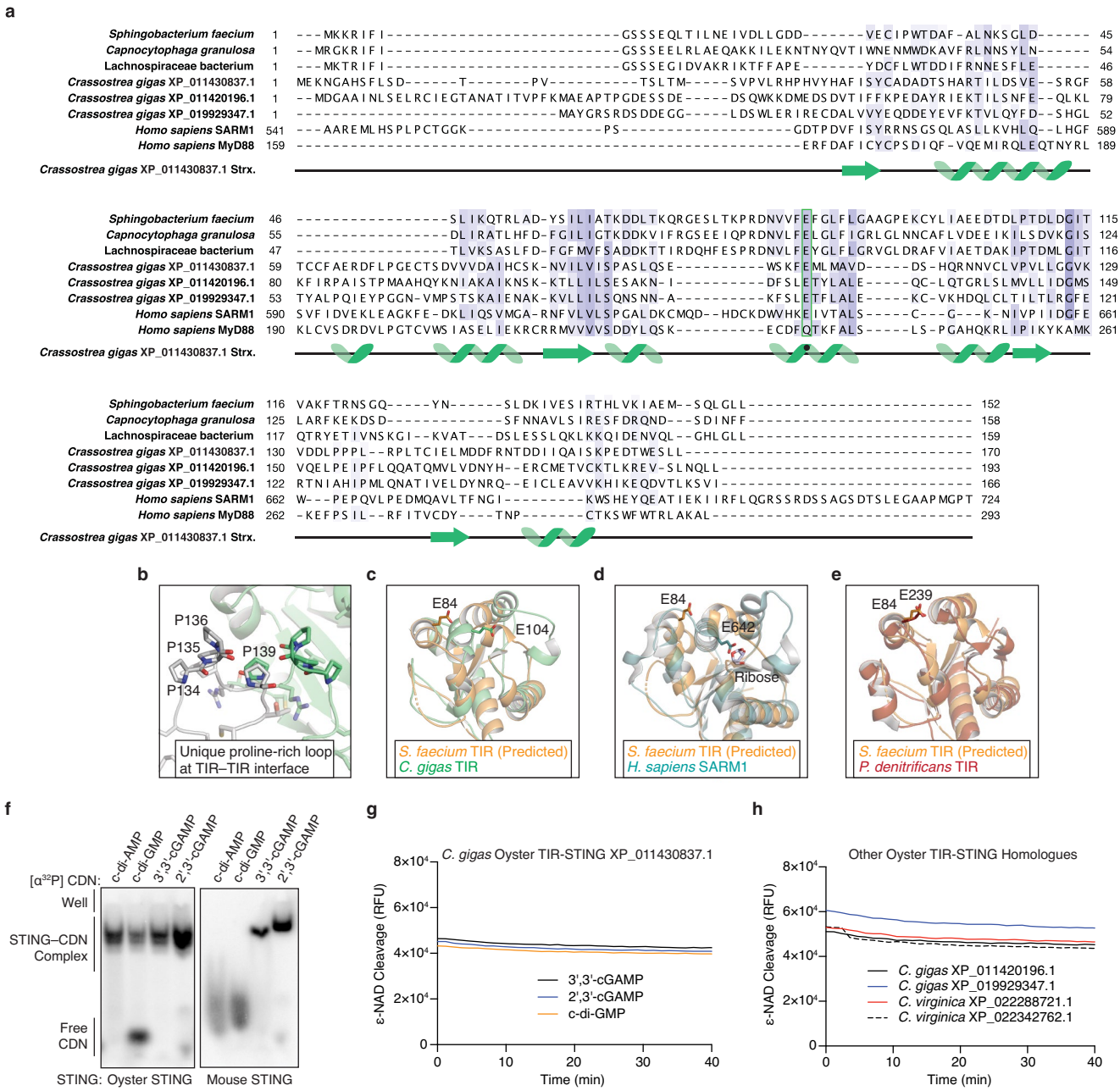

Extended Data Fig. 9 | Structural analysis of metazoan TIR–STING homologues. a, Structure-guided alignment of the TIR domain in oyster TIR–STING with reference bacterial and metazoan TIR-domain-containing proteins. SARM1 is an example of a human TIR domain that catalyses NAD^+ cleavage, and MyD88 is an example of a human TIR domain that signals through protein–protein interaction. The catalytic glutamate responsible for supporting NAD^+ cleavage is conserved at the same spatial position among bacterial and oyster TIRs but is mutated in MyD88 (green box). However, it is not currently possible to predict from structure or sequence alone whether TIR domains have enzymatic activity. **b**, Distinct from other TIR domain structures, the TIR domain in oyster TIR–STING contains a proline-rich loop region at the interface, suggesting a specific role in dimer stabilization. **c**, Superposition of a homology model of the *Sf*STING TIR domain with the TIR domain of oyster TIR–STING shows the predicted catalytic glutamates for both proteins occupy distinct locations in the TIR fold. **d**, Superposition of a homology model of the *Sf*STING TIR domain compared to the crystal structure of human SARM1 bound to ribose implies that different NAD^+ binding pockets may exist between bacterial and eukaryotic TIRs, as previously suggested[21]. **e**, Superposition of a homology model of the *Sf*STING TIR domain with the bacterial TIR domain from *Paracoccus denitrificans* shows a high degree of similarity. No crystal structures are available for bacterial TIR domains in an active state, preventing identification of a specific mechanism of catalytic activation. **f**, EMSA analysis of oyster TIR–STING and mouse STING demonstrates a wide preference for cyclic dinucleotide interactions and clear ability to recognize the mammalian cGAS product 2′,3′-cGAMP. Data are representative of three independent experiments. **g**, **h**, Oyster TIR–STING, which binds all tested cyclic dinucleotides, does not exhibit NAD^+ cleavage activity even at 10× the protein and ligand concentrations used to achieve robust activity with bacterial TIR–STING. We tested four other oyster TIR–STING homologues and observed no cyclic-dinucleotide-stimulated NAD^+ cleavage activity. These results support a potential switch in TIR-dependent protein–protein interactions to control downstream signalling similar to the TIR domain in human MyD88. Data are representative of two independent experiments.

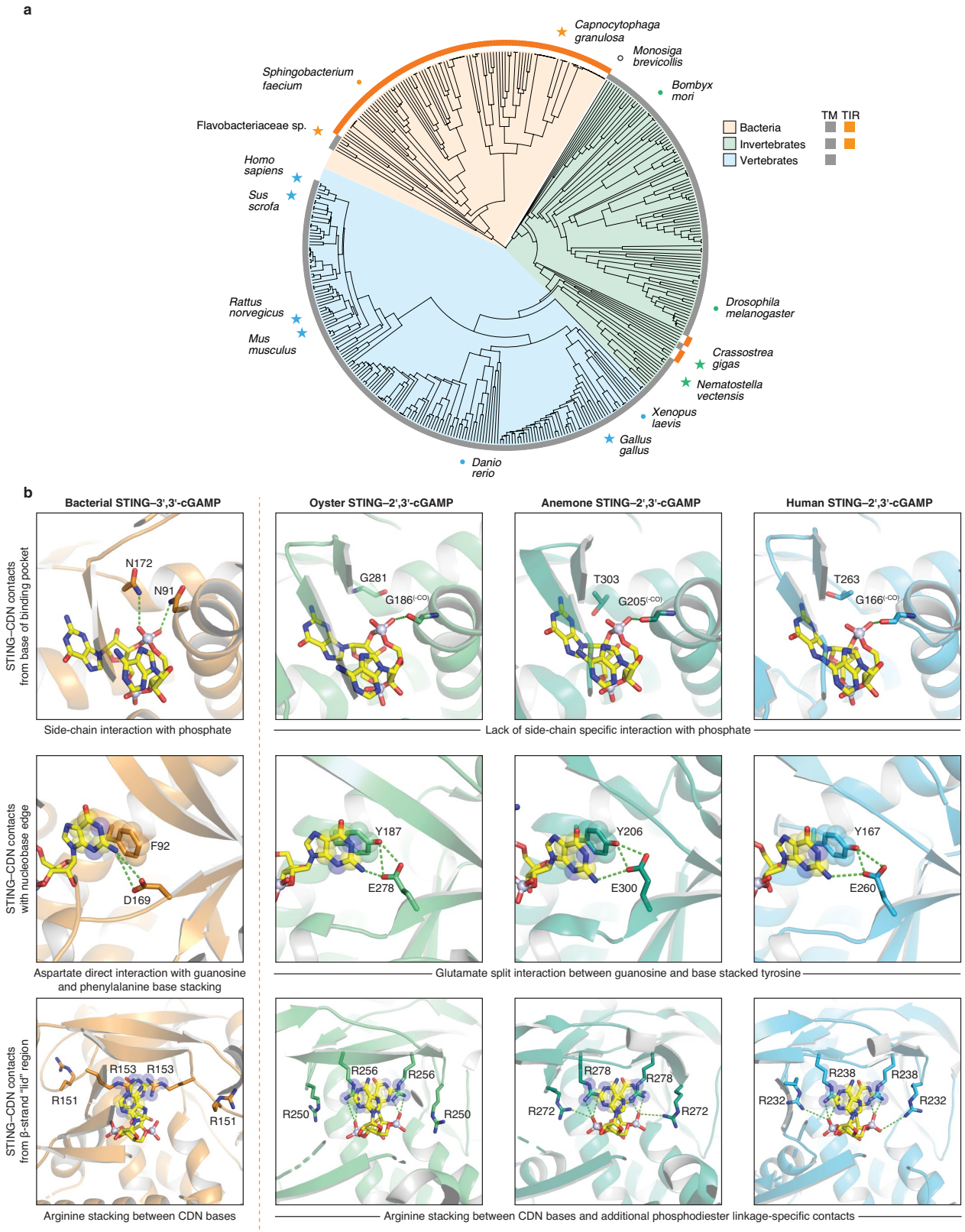

Extended Data Fig. 10 | See next page for caption.

Extended Data Fig. 10 | Structure-guided analysis of STING phylogenetic conservation and cyclic dinucleotide recognition. a, Structure-guided alignment and phylogenetic tree of STING proteins across bacterial and metazoan kingdoms. Bacterial STING homologues form a distinct cluster separate from all metazoan STING sequences, and are mostly represented by TIR–STING fusions. A single STING-domain containing protein was identified in the choanoflagellate *Monosiga brevicollis* (denoted as an open black circle, as this species is outside of the kingdom Metazoa); no STING-domain containing proteins were found in Archaea. TIR–STING fusions are rare in eukaryotes and cluster among invertebrate metazoans. No TIR–STING examples occur in vertebrates. Specific species of interest are highlighted to show the breadth of sequence diversity and stars mark proteins with available structures. **b**, Direct comparison of bacterial, oyster, anemone and human STING crystal structures reveals conservation of specific cyclic dinucleotide contacts and critical differences in phosphodiester linkage recognition. Stacking interactions formed with the cyclic dinucleotide nucleobase face, aromatic side chains at the top of the α-helix stem and arginine residues extending downward from the lid region are major conserved features shared between bacterial and metazoan STING proteins. Nucleotide-specific contacts are divergent between distinct STING structures, but notably the critical D169 guanosine N2-specific contact present in bacterial STING is conserved with a glutamic acid side chain in nearly all metazoan STING proteins. A critical feature absent in bacterial STING receptors is additional arginine-specific contacts to the phosphodiester backbone. The human STING R232 side chain contact, known to be critical for high-affinity interactions with 2′,3′-cGAMP, is conserved throughout metazoan STINGs, representing a unique adaptation not found within bacterial STING receptors. Bacterial STING–3′,3′-cGAMP (FsSTING), oyster STING–2′,3′-cGAMP (*C. gigas*), sea anemone STING–2′,3′-cGAMP (*N. vectensis* PDB 5CFQ)[8], human STING–2′,3′-cGAMP (*H. sapiens* PDB 4KSY)[7].

nature research

Corresponding author(s): Philip J. Kranzusch

Last updated by author(s): Aug 17, 2020

Reporting Summary

Nature Research wishes to improve the reproducibility of the work that we publish. This form provides structure for consistency and transparency in reporting. For further information on Nature Research policies, see our Editorial Policies and the Editorial Policy Checklist.

Statistics

For all statistical analyses, confirm that the following items are present in the figure legend, table legend, main text, or Methods section.

n/a	Confirmed	
☐	☒	The exact sample size (*n*) for each experimental group/condition, given as a discrete number and unit of measurement
☒	☐	A statement on whether measurements were taken from distinct samples or whether the same sample was measured repeatedly
☐	☒	The statistical test(s) used AND whether they are one- or two-sided *Only common tests should be described solely by name; describe more complex techniques in the Methods section.*
☒	☐	A description of all covariates tested
☒	☐	A description of any assumptions or corrections, such as tests of normality and adjustment for multiple comparisons
☐	☒	A full description of the statistical parameters including central tendency (e.g. means) or other basic estimates (e.g. regression coefficient) AND variation (e.g. standard deviation) or associated estimates of uncertainty (e.g. confidence intervals)
☒	☐	For null hypothesis testing, the test statistic (e.g. *F*, *t*, *r*) with confidence intervals, effect sizes, degrees of freedom and *P* value noted *Give P values as exact values whenever suitable.*
☒	☐	For Bayesian analysis, information on the choice of priors and Markov chain Monte Carlo settings
☒	☐	For hierarchical and complex designs, identification of the appropriate level for tests and full reporting of outcomes
☒	☐	Estimates of effect sizes (e.g. Cohen's *d*, Pearson's *r*), indicating how they were calculated

Our web collection on statistics for biologists contains articles on many of the points above.

Software and code

Policy information about availability of computer code

Data collection	No software was used for data collection.
Data analysis	Phenix 1.17, Coot 0.8.9, PyMOL 2.3.4, GraphPad Prism 8.4.2, RELION 3, ASTRA 7, ImageQuant 5.2

For manuscripts utilizing custom algorithms or software that are central to the research but not yet described in published literature, software must be made available to editors and reviewers. We strongly encourage code deposition in a community repository (e.g. GitHub). See the Nature Research guidelines for submitting code & software for further information.

Data

Policy information about availability of data

All manuscripts must include a data availability statement. This statement should provide the following information, where applicable:

- Accession codes, unique identifiers, or web links for publicly available datasets
- A list of figures that have associated raw data
- A description of any restrictions on data availability

Data that support the findings of this study are available within the article and its Extended Data and Supplementary Tables. Integrated Microbial Genomes (IMG) database accessions are listed in Extended Data Figure 1 and Protein Data Bank (PDB) database accessions are listed in each figure legend. Coordinates and structure factors of FsSTING–3',3'-cGAMP, CgSTING, oyster TIR-STING, oyster TIR-STING–2',3'-cGAMP, FsCdnE, and CgCdnE have been deposited in PDB under accession codes 6WT4, 6WT5, 6WT6, 6WT7, 6WT8, and 6WT9.

Field-specific reporting

Please select the one below that is the best fit for your research. If you are not sure, read the appropriate sections before making your selection.

☒ Life sciences ☐ Behavioural & social sciences ☐ Ecological, evolutionary & environmental sciences

For a reference copy of the document with all sections, see nature.com/documents/nr-reporting-summary-flat.pdf

Life sciences study design

All studies must disclose on these points even when the disclosure is negative.

Sample size	No sample size calculation was performed. Sample sizes for biochemical and bacterial growth experiments were selected based on widely adopted protocols in the field.
Data exclusions	No data were excluded from the analyses.
Replication	All experiments were performed with independent replicates as described in the figure legends.
Randomization	X-ray crystal structures were refined with a randomly selected R-free reflection set based on automatic selection in Phenix 1.17. Randomization is not relevant to the biochemical and bacterial growth experiments described in this work.
Blinding	Data were not blinded. Blinding is not relevant to the structural, biochemical, or bacterial growth experiments described in this work as subjective analyses were not performed.

Reporting for specific materials, systems and methods

We require information from authors about some types of materials, experimental systems and methods used in many studies. Here, indicate whether each material, system or method listed is relevant to your study. If you are not sure if a list item applies to your research, read the appropriate section before selecting a response.

Materials & experimental systems

n/a	Involved in the study
☒	☐ Antibodies
☒	☐ Eukaryotic cell lines
☒	☐ Palaeontology and archaeology
☒	☐ Animals and other organisms
☒	☐ Human research participants
☒	☐ Clinical data
☒	☐ Dual use research of concern

Methods

n/a	Involved in the study
☒	☐ ChIP-seq
☒	☐ Flow cytometry
☒	☐ MRI-based neuroimaging